AN ASSESSMENT OF THE CORROSION RESISTANCE OF POWDER SPRAYED TITANIUM COATINGS

A thesis
submitted in fulfilment
of the requirements for the degree
of
Master of Engineering
at
The University of Waikato
by
EVAN GUY GRAY PROBERT

The University of Waikato
2010

Abstract

Aluminium and stainless steels are susceptible to pitting corrosion in sea water. Mild steel is susceptible to corrosion in general. Titanium however, has good corrosion resistance in chloride solutions and thus is not susceptible to pitting in sea water. The following is an assessment of the corrosion resistance of Titanium powder coatings. Potentiostatic electrochemical experiments were carried out on three substrates (stainless steel, mild steel and Aluminium) coated using two spray methods (plasma and HVOF). A discussion of the results was given with reference to the polarisation curves that were created, SEM images, XRD results, estimates of porosity, and Pourbaix diagrams. It was concluded that the plasma coating provides the best corrosion resistance due to the fact that it had less porosity than HVOF and that it is made up of Titanium oxides. Also, the corrosion mechanism for the coatings is pitting of the substrates at the end of pores. The extent of this is far greater for the HVOF than the plasma coating. It was found that features found in the polarisation curves for the substrates are present in the curves for coatings. This is more evident in the HVOF polarisation curves. Mild steel benefited the most from the Titanium coatings compared to the substrate (more so for the plasma coating). Finally, the plasma coating improves the substrate based on corrosion rate and thermodynamics, except for Aluminium which remains the same thermodynamically.

,

Acknowledgments

The following people have provided assistance in the duration of the Masters of Engineering:

The staff at Holster Engineering

Brian Gabbitas

Yuanji Zhang

Asma Salman

Workshop staff

Jannine Rhodes

Wendy Jackson

Stella Raynova

Helen Turner

Table of Contents

List of Figures

List of Tables

1.0 Introduction

Aluminium and stainless steels are susceptible to pitting corrosion in sea water. Mild steel is susceptible to corrosion in general. Titanium however, has good corrosion resistance in chloride solutions and thus is not susceptible to pitting in sea water [1]. It is with this in mind that research into Titanium coatings is carried out. The following is an investigation into the corrosion resistance of Titanium coatings. Details of potentiostatic electrochemical experiments for three different substrates (mild steel, stainless steel and Aluminium) coated by Plasma and HVOF (High Velocity Oxygen Fuel) spraying methods are detailed following a discussion of the relevant literature. The results of the experiments are then given; cross referenced by substrate and spraying method. This leads to a discussion of the results followed by the conclusion drawn from the discussion and some recommendations for future work.

2.0 Literature Review

Titanium has very good corrosion resistance in most environments so there are a large number of studies into protecting materials with Titanium and Titanium based coatings

There are multiple studies into the corrosion resistance of TiN coatings; one such study was carried out by P.M. Perillo [2]. The study looked at different coating types; including Ti, Ti-TiN and TiN coatings. It was found that the corrosion resistance of Ti coatings was greater than that of TiN coating with a Ti intermediate coating, and that in turn had greater resistance than just a TiN coating. P.M. Perillo also compared the corrosion resistance of TiN coatings of different thickness. It was found that corrosion resistance increases with increasing coating thickness. This was due to thicker coatings having fewer defects; and thus reducing the chance of galvanic attack.

Another study into the corrosion resistance of TiN coatings was done by Mao, Ma, Wang and Sun [3]. Their study involved comparing corrosion resistance of composite coatings (TiN based) made from powders prepared by both mixed and sintering methods. They found that the coating containing sintered powder had a more porous cross-section than that of the mixed powder. This was because the mixed powder contained Cr, which melts during thermal spraying and fills the pores. It was also found that the mixed powder coating had better corrosion resistance. This was mainly due to the addition of Cr in the coating; due to both its corrosion resistant properties and the aforementioned pore filling property.

Baba and Hatada investigated the effect of ion-beam-assisted deposition on the corrosion behaviour of TiN coatings [4]. The experiment involved the study of Ti implantation and the application of a thin Ti film on the surface of the substrate prior to TiN coating, in relation to its corrosion resistance. They found that Ti implantation gave rise to a well mixed layer between coating and substrate. They also found that corrosion resistance increased when the surface of the substrate was implanted with Ti and a thin layer of Ti was applied before the TiN.

A similar study was carried out by Wu et al. [5]. They altered the surface characteristics of a magnesium alloy substrate by bombarding the surface with Nitrogen. The substrate was then coated with Ti. The corrosion characteristics of this were compared to the substrate and an untreated substrate with Ti coating. The study found that the surface altered substrate with Ti coating provided better corrosion resistance than that of the unaltered substrate with Ti coating. This was due to many things, including the fact that the surface treatment produced a better bond between the coating and the substrate. The Nitrogen bombardment also cleaned the surface of the substrate, thus reducing the surface activity. The surface treatment also acted as a barrier to corrosion once the corrosive medium reaches the substrate through the pores in the coating.

Another study into Ti coatings was carried out by Hong-Ren et al. [6]. In this study the corrosion resistance of Ti coating was compared to that of pure Ti. It was determined that the corrosion was more aggressive for the Ti coating than the pure Ti. This was attributed to the coating having a much more active surface (due to the porous surface layer). To reduce the activity of the surface, the coating was polished, and the corrosion resistance was tested. It was found that the polished coating exhibited better corrosion resistance than that of the unpolished coating, but not equal to that of the pure Ti. This discrepancy was caused by poor bonding between deposited particles.

2.1 Electrodes and Electrolytes

The choice of reference electrode in the aforementioned literature is a choice between two types. Baba and Hatada, and Mao et al. used a Ag/AgCl in their experiments, while Hong-Ren et al., Wu et al., and Perillo used a saturated calomel electrode [2-6]. The choice of which electrode to use could be as simple as the desire to (or not to) use an electrode that contained Mercury (saturated calomel electrode). There appears to be no choice in the counter electrode to use. All the studies into Ti coatings used a Platinum counter electrode (except for Baba and Hatada, who did not specify which counter electrode they used). The form of the Platinum electrode varies, however, including wire, pole and sheet. The choice of form may be due to cost, as any other reason is not obvious. The choice of electrolyte seems to be a choice between 3.5% NaCl and 5% H_2SO_4 (except Hong-Ren et al. that used seawater). The decision of which electrolyte could be due to the desire to simulate sea water (NaCl).

3.0 Experimental Details

3.1 Powder Normalization

Powder coatings using Titanium powder deposited by High Velocity Oxygen Fuel (HVOF) and Plasma spraying were made at Holster Engineering. On the first visit to Holster Engineering it was found that the Ti powder would not flow and thus spraying was not possible. The powder then needed to be normalized using poly vinyl acetate (PVA) solution. The solution was created by heating up distilled water to 70°C using a hotplate, then adding PVA solid and a magnetic stirrer. The solution was then mixed until the PVA was dissolved. The appropriate concentration of PVA solution was found by trial and error. The first concentration trialled was 2% (by weight) PVA solution. 4g of PVA was mixed with 200ml of distilled water to create the solution. The solution was then added to Ti powder at a ratio of 10ml per 100g of powder, and then mixed. The powder was put in an oven overnight at 80°C. Then, the powder was sifted through a 106 micron sieve. When the powder would not fit through the sieve, it was forced through so that all the powder was less than 106 microns. A small amount of the powder was put into a flow meter to test for flow.

The 2% PVA solution did not produce flowing powder, so 3% solution was tried. The powder flowed, but to make sure that 3% solution was the correct solution, 4% was tried. The powder did not flow when mixed with 4% solution, so 3% PVA solution was used. Figure 1 shows the difference between the treated and untreated powders. 600ml of 3% PVA solution was made and 500g of powder was treated for use in spraying.

Figure 1: The untreated powder (left) and the powder treated with 3% PVA solution (right)

3.2 Spraying

Three types of substrates were brought to Holster Engineering for spraying. The substrates were 601 ingot Aluminium, 316 Stainless Steel, and Mild Steel. Each of the substrate was sprayed using Plasma and HVOF spray methods. Before spraying the substrates were sand blasted. The parameters of the equipment can be seen in table A1 (in appendix A).

3.3 Electrochemical Testing

All electrochemical experiments were carried out using a Radiometer PGP201 potentiostat/gavanostat. The reference electrode in all experiments was a Ag/AgCl (sat KCL solution) and the auxiliary electrode was a Pt wire. The electrolyte in all experiments was a 3.5% NaCl solution (by weight). This was made in 1600ml batches (enough for two experiments) by mixing 1600 ml of distilled water with 56g of NaCl. The working electrodes were obtained from the bulk material by cutting a strip 1.5cm wide using a band saw. The strips were then cut into 5cm long lengths. The aim of the first several experiments was to become familiar with the equipment and methods.

The first experiment was a sample of stainless steel coated by Plasma spraying method, dubbed 1SP. A 1cm^2 area was masked off using wax. The wax was melted using a hot plate and the sample dipped into it. Electrical isolation was tested using a digital multimeter. The working electrode was attached to the working electrode lead by drilling a hole in the electrode and putting a nut and bolt through it. Figure 2 shows the first two working electrodes with the bolts.

Figure 2: 1SP (left) and 2SP (right) with attachment bolt through them.

The alligator clip on the lead was then attached to the bolt. The three electrodes were submerged in the electrolyte, making sure that the 1cm^2 area was the only part of the working electrode exposed to the electrolyte. The electrodes were allowed to sit in the electrolyte for 30mins before the experiment started, to allow the cell to reach steady state. The voltage of the potentiostat in the experiment was changed manually in 10mV steps, starting at -1000mV (-1V). After each step the current reading was allowed to reach steady state. Figure 3 shows the experimental setup and figure 4 shows the placement of the electrodes.

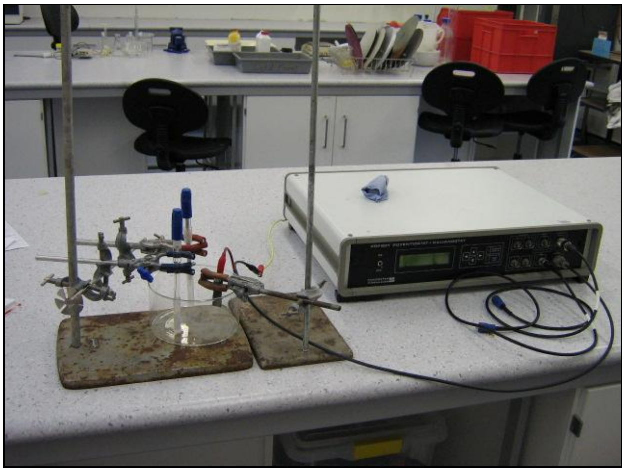

Figure 3: Experimental setup.

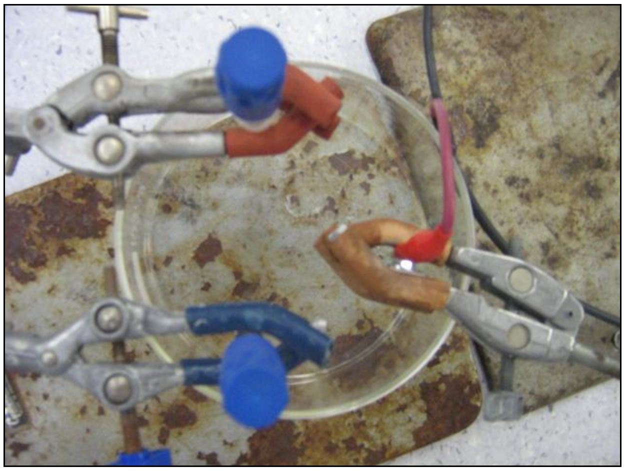

Figure 4: The placement of the electrodes

At -50mV the auxiliary electrode started bubbling and the current became very large and would not stop increasing. The experiment was then aborted and literature was consulted as to what went wrong.

2 recommendations were found in literature [7]:

1. The auxiliary electrode should have a larger surface area than the working electrode.

2. The reference electrode should be right next to the working electrode.

The surface area of the auxiliary electrode was calculated to be 35.7mm^2.

The second experiment was with another sample of stainless steel coated using Plasma spraying method, dubbed 2SP. The sample was masked off with wax, with an exposed area of 0.5 x 0.5cm (25mm^2). The electrodes were submerged in the electrolyte and allowed to sit for ten minutes. The step size was increased to 40mV for the experiment, due to the fact that the first experiment took in excess of 4 hours to get to less than half of the desired experiment. Figure 5 shows the revised placement of the electrodes. At 0mV the auxiliary electrode bubbled and the current took off. The experiment was aborted.

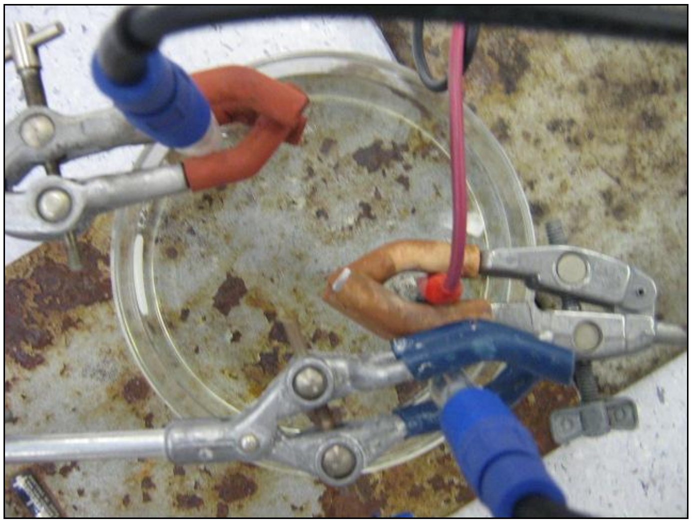

Figure 5: The revised placement of the electrodes.

After two failed experiments, the third experiment was to determine if the method or equipment were flawed. The working electrode was a consolidated Ti powder sample, and was dubbed 1T. The sample was cut with a wire cutter to 1.5cm wide and 5cm long. The surfaces of the sample were ground using a grinding wheel. An area of $1cm^2$ was masked off using wax. A picture hanger was modified so that the working electrode lead could be attached to the electrode. The electrode was then tested for electrical continuity using a digital multimeter. A complete experiment was preformed from -1000mV to 1000mV, so the equipment was not faulty.

For the next group of experiments several changes were made to the experiment. First, the exposed area of the working electrode was $1cm^2$ again. This was because it was difficult to mask off the smaller area and it was difficult to cut the smaller area for use under the scanning electron microscope. Second, the material used to mask off the samples was changed from wax to nail polish. This was done because it was difficult to accurately apply the wax and almost impossible to guarantee complete coverage due to the transparent nature of the wax. Black nail polish was used so that complete coverage could be confirmed.

Third, readings were taken of the current at 1min after each 40mV step. This was due to the fact that the 1T experiment took in excess of 9 hours to complete (and several of the final measurements were skipped). In addition to the 10mins before the start of the experiment, the first measurement was taken after 10mins to allow the experiment to reach steady state once the experiment had started. The working electrodes that were thin enough were attached directly to the lead via the alligator clip (stainless steel and mild steel); the others were attached using the modified picture hanger and the alligator clip (Aluminium).

VoltaMaster 4 software for controlling the potentiostat/galvostat was also used to obtain potentiostatic measurements. The experiments reported earlier in this section were repeated using the software. For each experiment the scan rate was set to 1mV/sec. A period of 10mins was still observed before the experiment was started and the electrolyte was still NaCl 3.5% by weight solution. The methods of masking and attaching the samples to the leads remained the same. Figure 6 shows the new experimental setup.

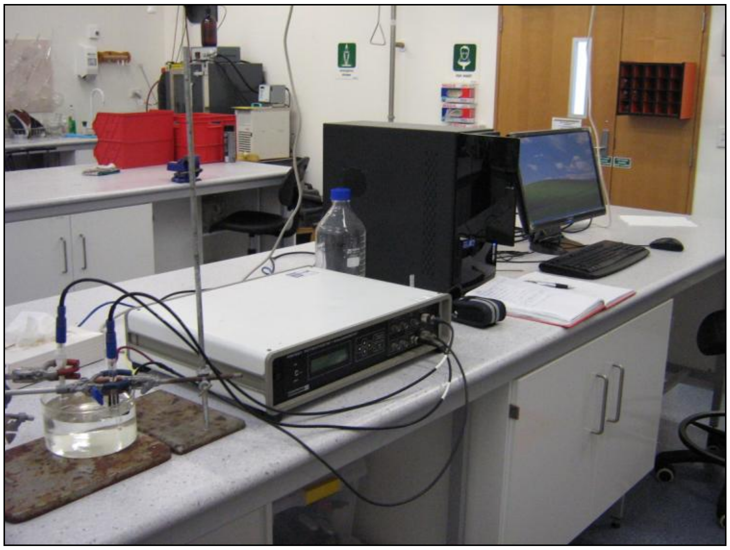

Figure 6: Experimental setup for the computer controlled experiments.

For all of the aforementioned electrochemical experiments the working electrode was weighed before and after the experiment (with masking). Prior to masking the working electrodes, they were rinsed in distilled water and degreased with ethanol. After the experiment all three of the electrodes were rinsed with distilled water. The temperature of the electrolyte was taken before each experiment and the electrolyte was discarded after each experiment. Table A2 (in appendix A) shows the details of the working electrodes that were used in the electrochemical experiments.

3.4 Sample Preparation for the Scanning Electron Microscope (SEM)

Corroded samples were cut through the exposed area using a band saw. They were then mounted using liquid resin at a ratio of 4.44:1 (epoxy resin: epoxy hardener). The mixture was poured over the samples in a mould and left over night to harden. The following morning the samples were ground and polished. Grinding was carried out from P120 to P4000 in stages, rotating the sample 90° after each stage. When the scratches from the previous stage were gone; the sample was moved to the next stage. The samples were then polished with 3µm diamond.

3.5 Second Spraying Session

To establish the density of the Plasma and HVOF coatings, a second spray session was carried out. Two, almost identical pieces of mild steel were used. One was labelled “A” and was sprayed using Plasma, and one was labelled “B” and sprayed using HVOF. The parameters in table A1 (in appendix A) were used for the spraying.

3.6 X-Ray Diffraction (XRD)

A sample of both Plasma and HVOF on stainless steel were examined by XRD. Samples were approximately 1.5 x 1.5cm. Peaks were assigned species using a known database.

4.0 Results

4.1 Experimental Parameters

Table A3 (in appendix A) shows the measurements taken before and after each experiment. It can be seen that the temperature has a range of 21.9±2.7°C. The dramatic difference in time taken between the different methods (manual, manual with a time limit at each step, and computer driven) can also be seen (1T compared to 3SP and 4SP respectively). The weight gain/loss of the samples can be seen in figure 7; which summarises the weight data in Table A3. Generally, it can be seen that the bare substrates have metal loss in the experiments. Also, the HVOF coated samples seem to have about the same metal loss as the bare substrates. The plasma coated samples however, generally have a metal gain as a result of the experiments.

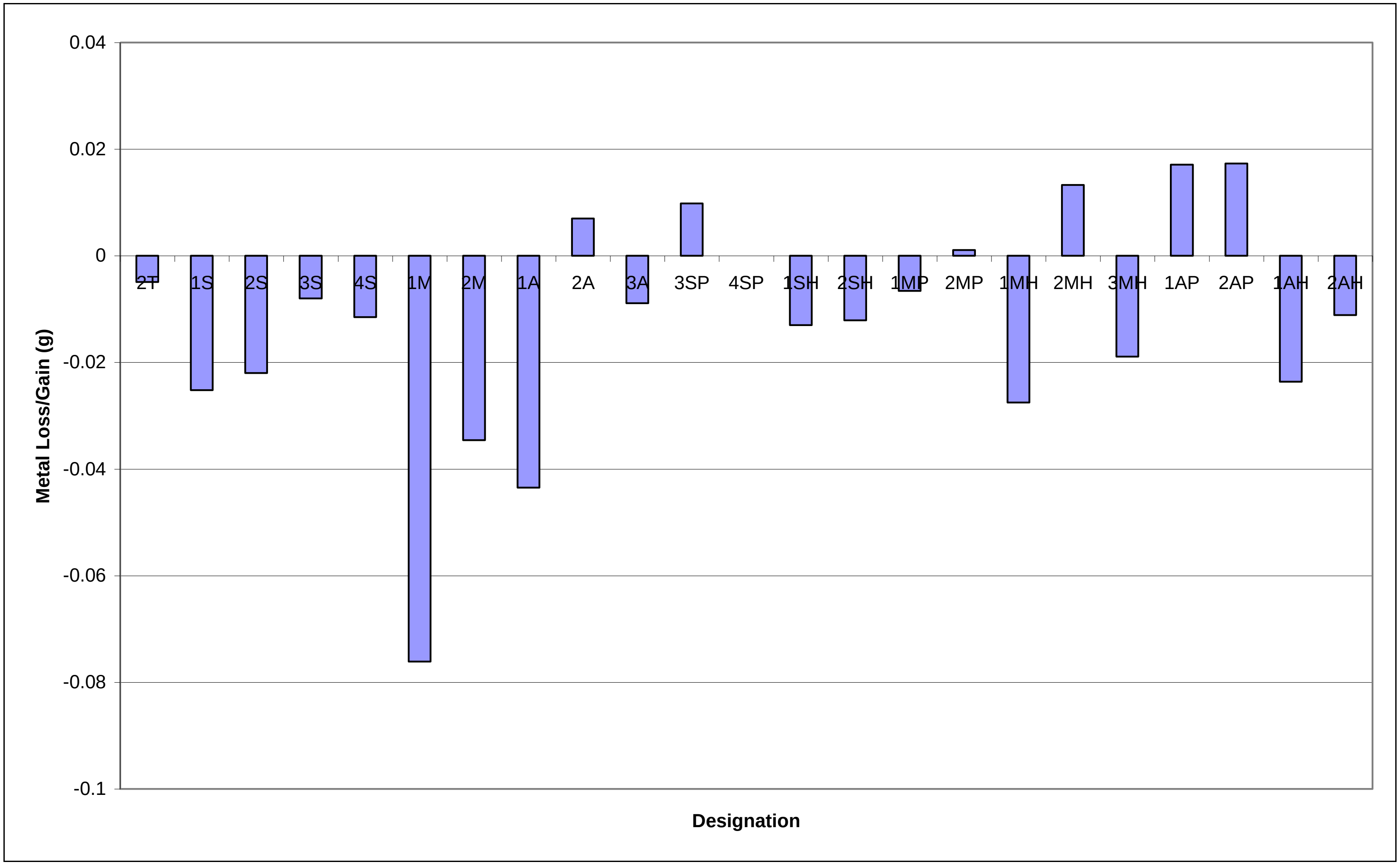

Figure 7: Graph of metal gain or loss for the different designations.

4.2 Observations

Table A4 (in appendix A) shows the observations that were made during the experiments. It can be extrapolated that Aluminium has the most violent corrosion of the three substrates. Mild steel appeared to lose the most metal into the solution. It is also important to note that the Platinum electrodes glass casing broke during the setup of the 3A experiment. The part of the electrode exposed to the electrolyte was still intact and the electrode still worked properly.

4.3 Electrochemical Experiments

Figures 8 - 20 show the results of the electrochemical experiments. Figures 8 – 13 show the results cross referenced by substrate type. It can be seen that for all of the substrates the results give the plasma coating as being the lowest current density followed by HVOF coating and bare substrates. Figures 14 – 17 show the results cross referenced by coating type. It can be seen that the curves have relatively the same placement in respect to one another for both the Plasma and HVOF coatings. Figure 15 has slightly different placement of the curves. Figures 18 and 19 show the results for the bare substrates and consolidated Titanium. The corrosion resistance in order of best to worse appears to be Titanium, stainless steel, mild steel and Aluminium. Figure 20 shows the results of the different methods of carrying out the experiments. It appears that for every successive method; the current density increases.

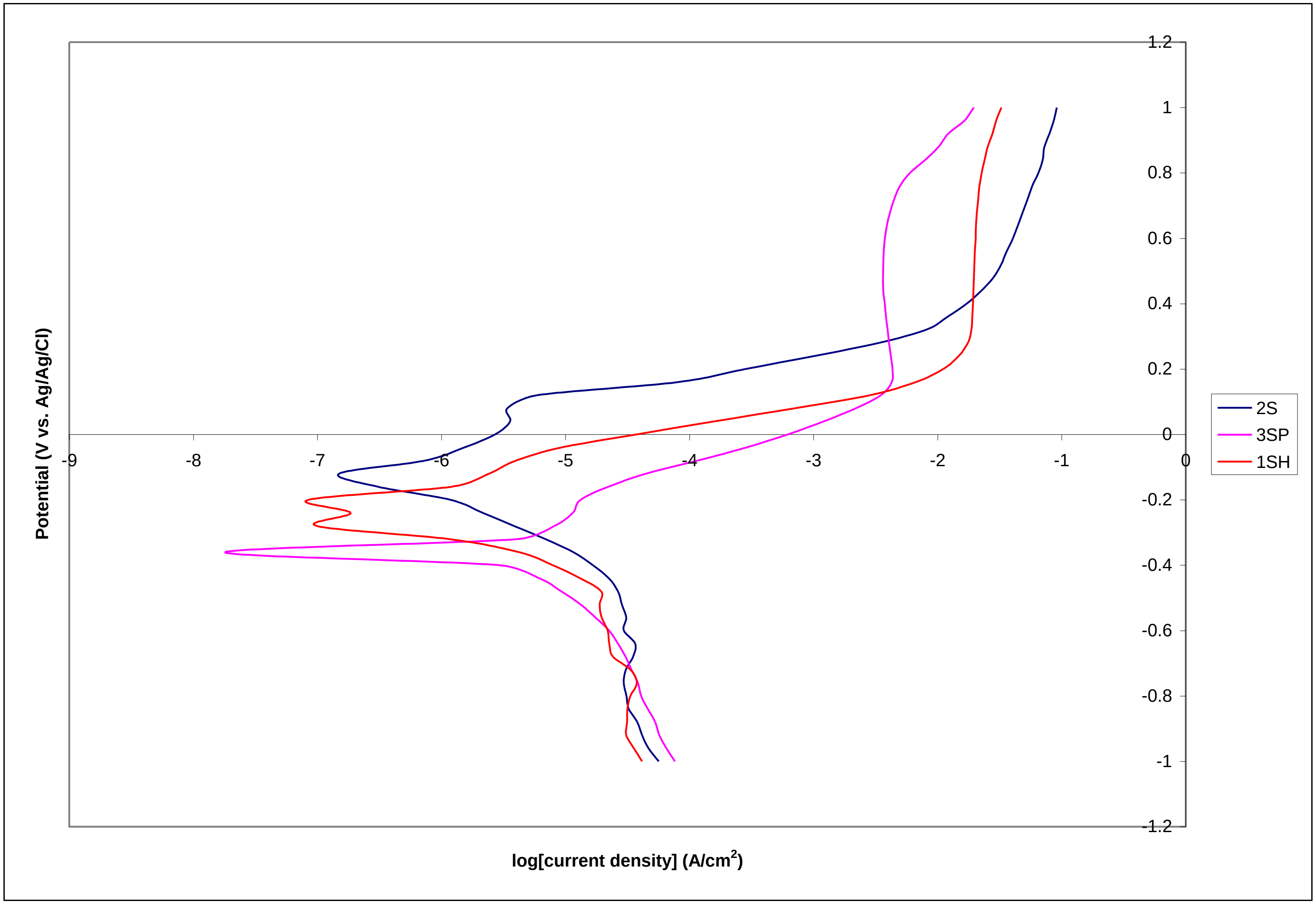

Figure 8: Graph of stainless steel substrate for the manual experiments.

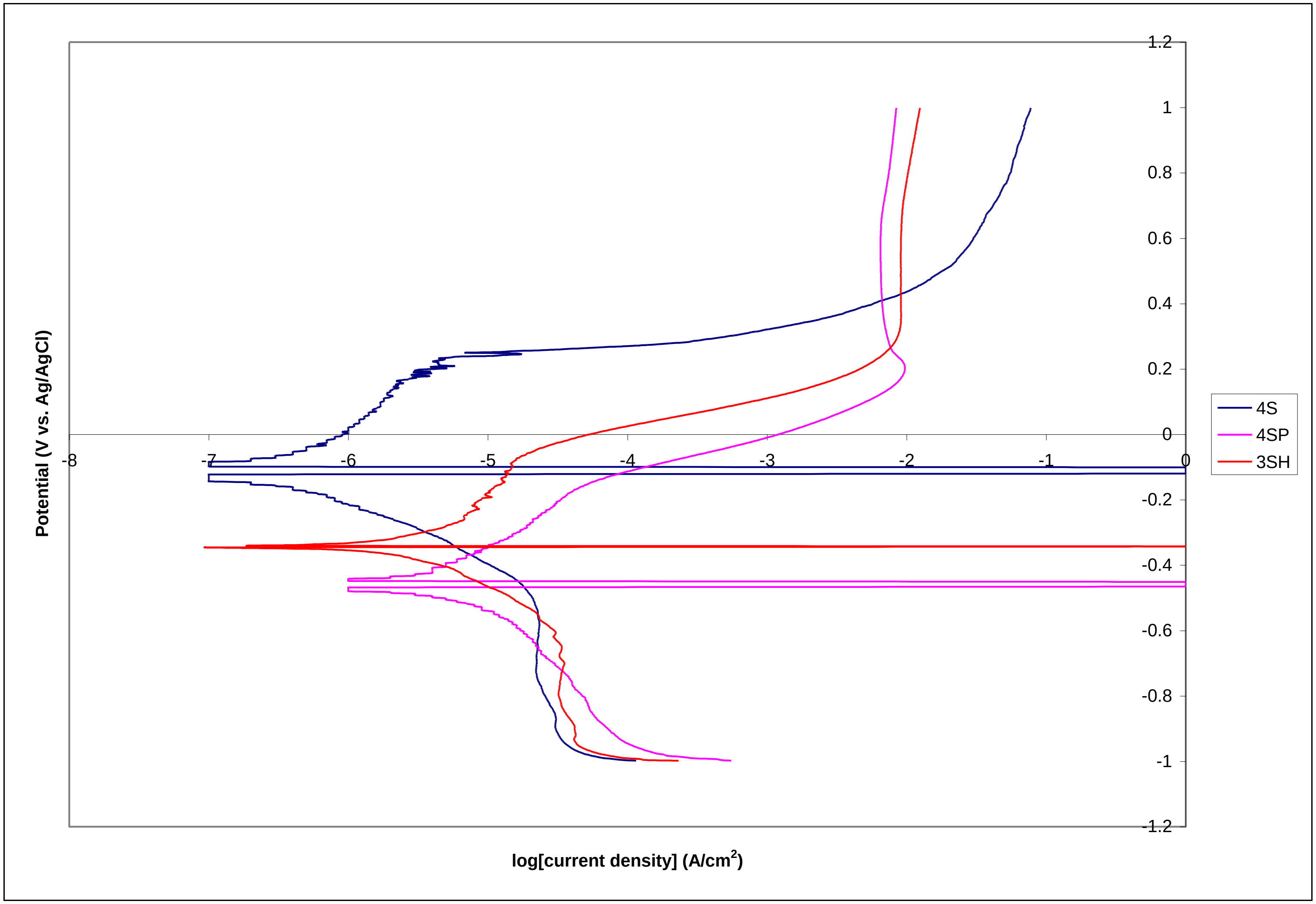

Figure 9: Graph of stainless steel substrate for the computer controlled experiments.

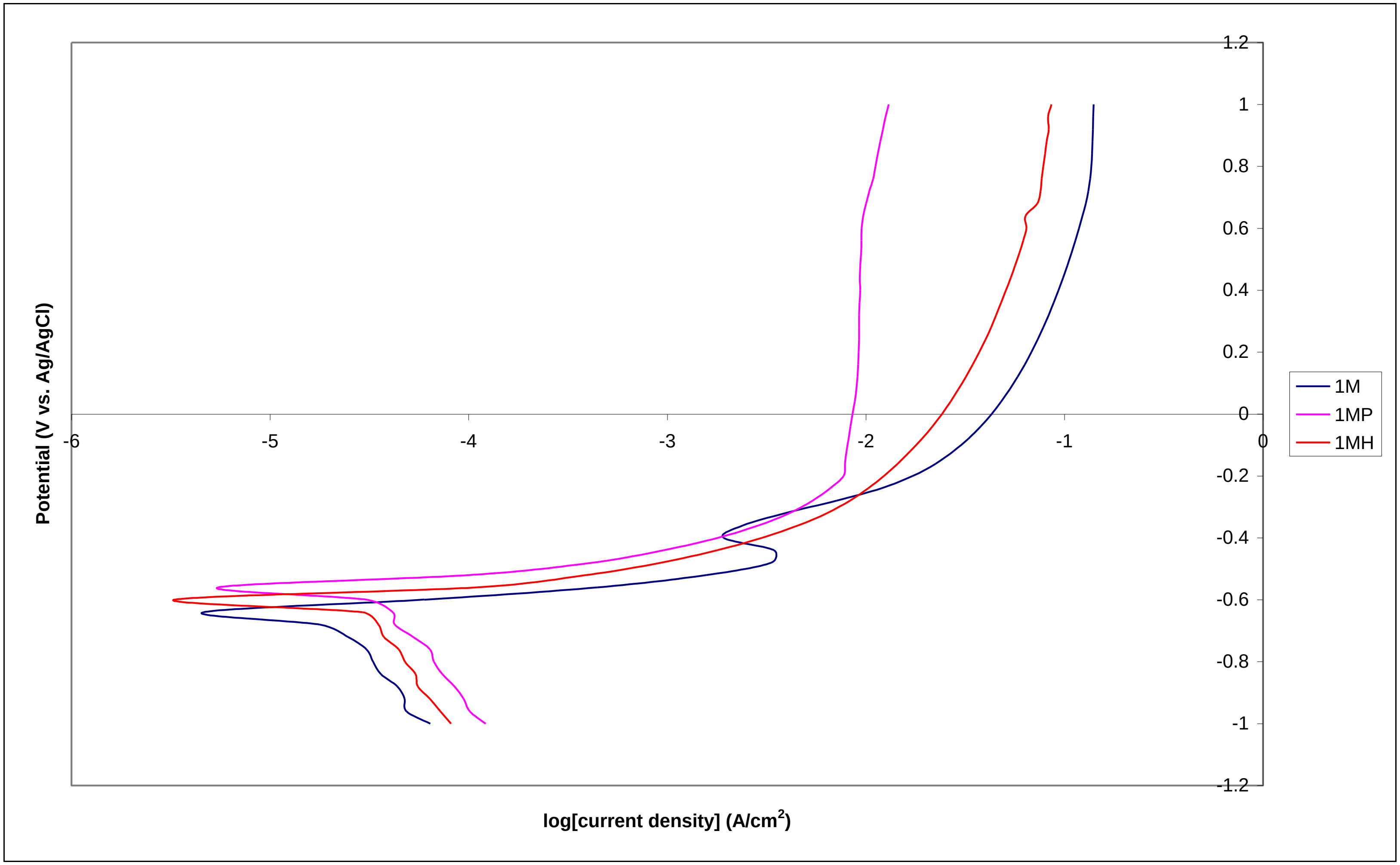

Figure 10: Graph of mild steel substrate for the manual experiments.

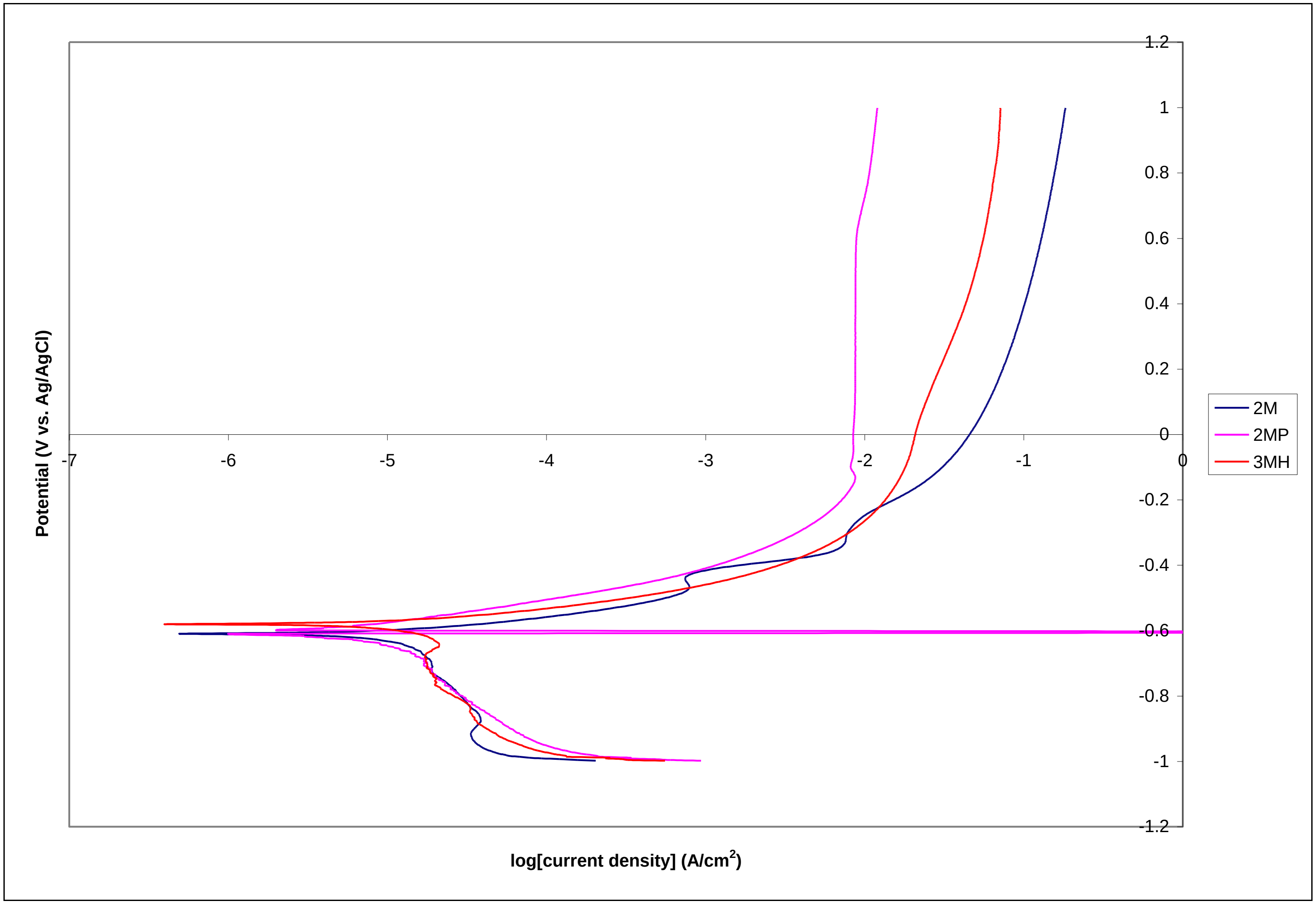

Figure 11: Graph of mild steel substrate for the computer controlled experiments.

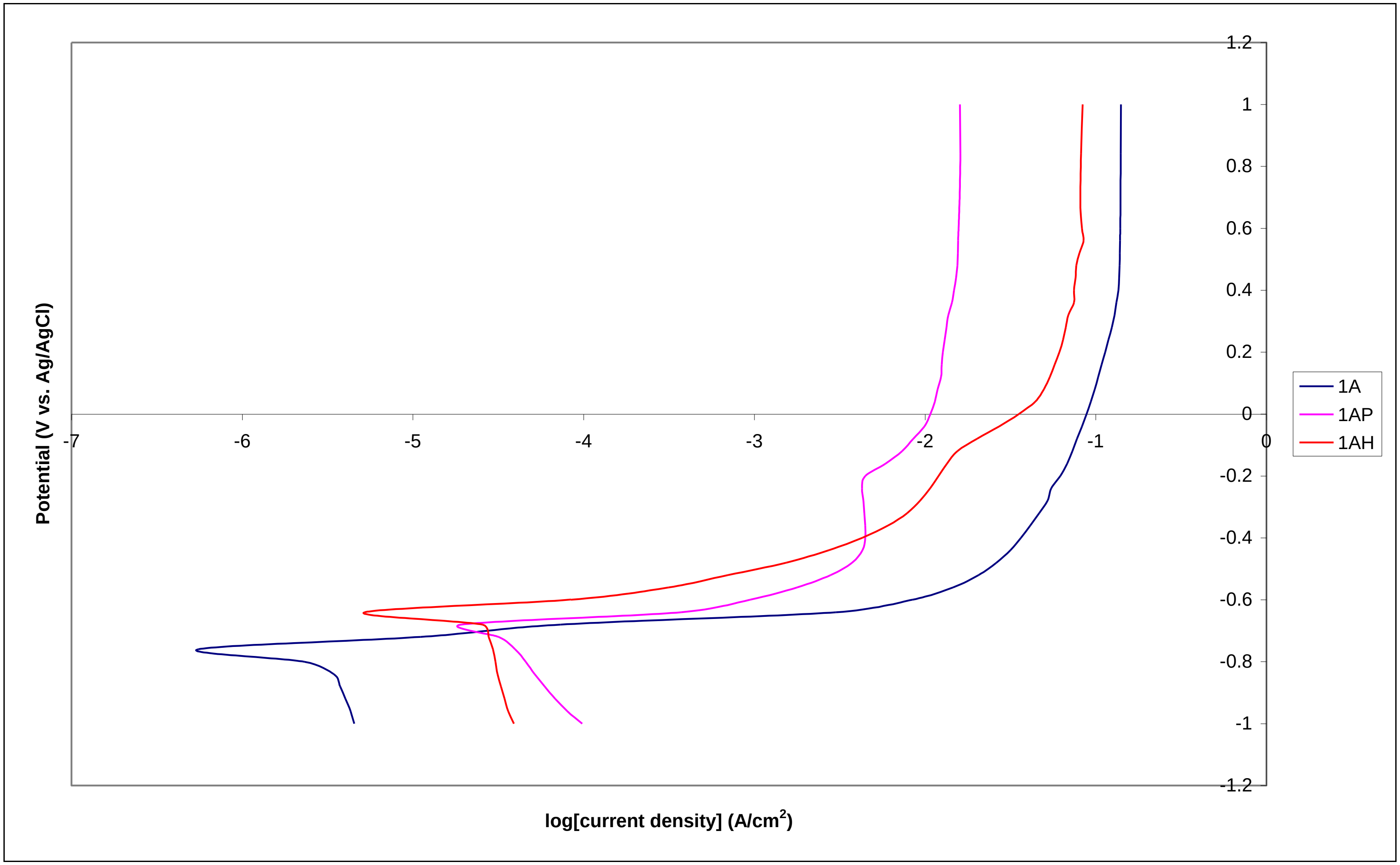

Figure 12: Graph of Aluminium substrate for the manual experiments.

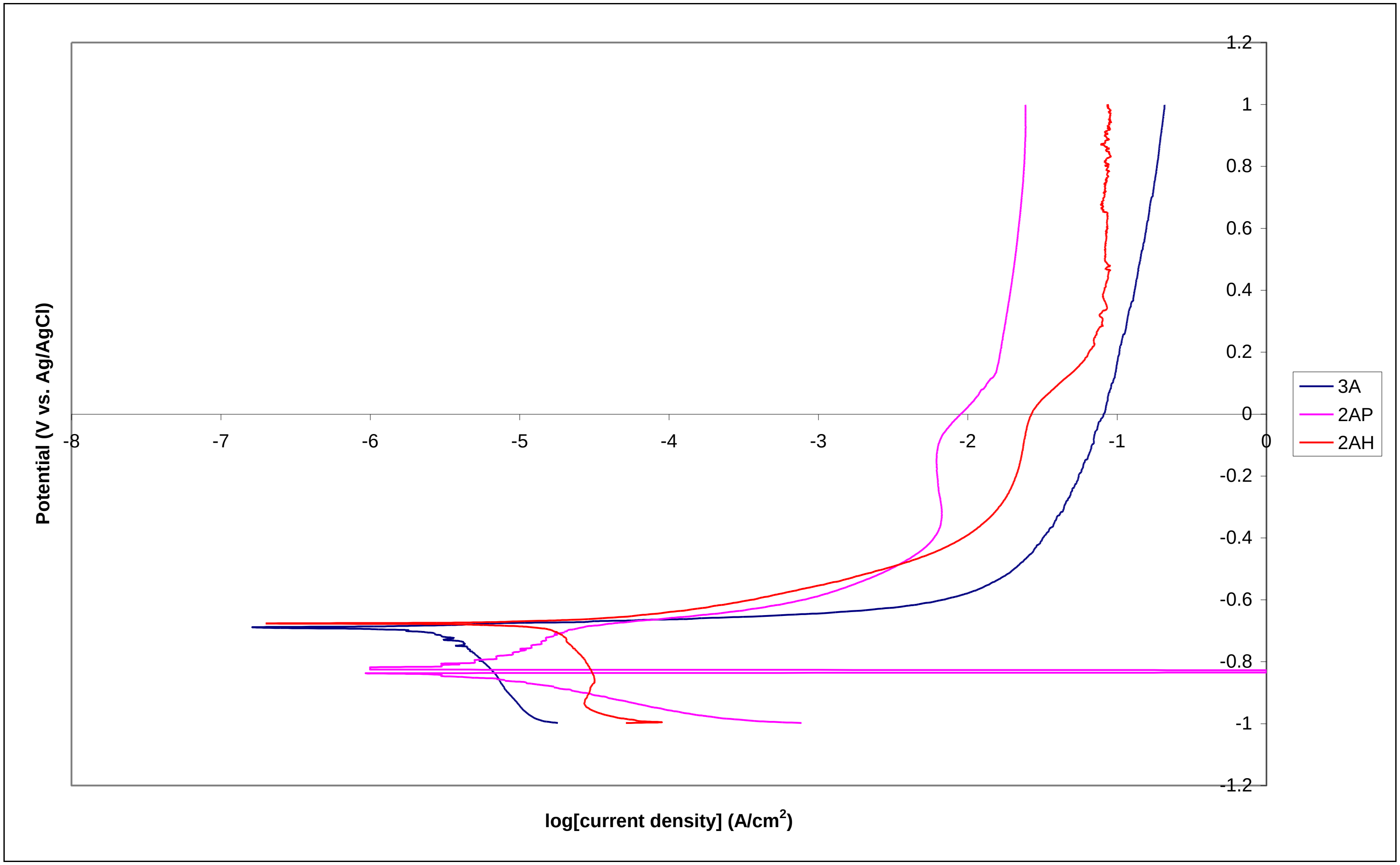

Figure 13: Graph of Aluminium substrate for the computer controlled experiments

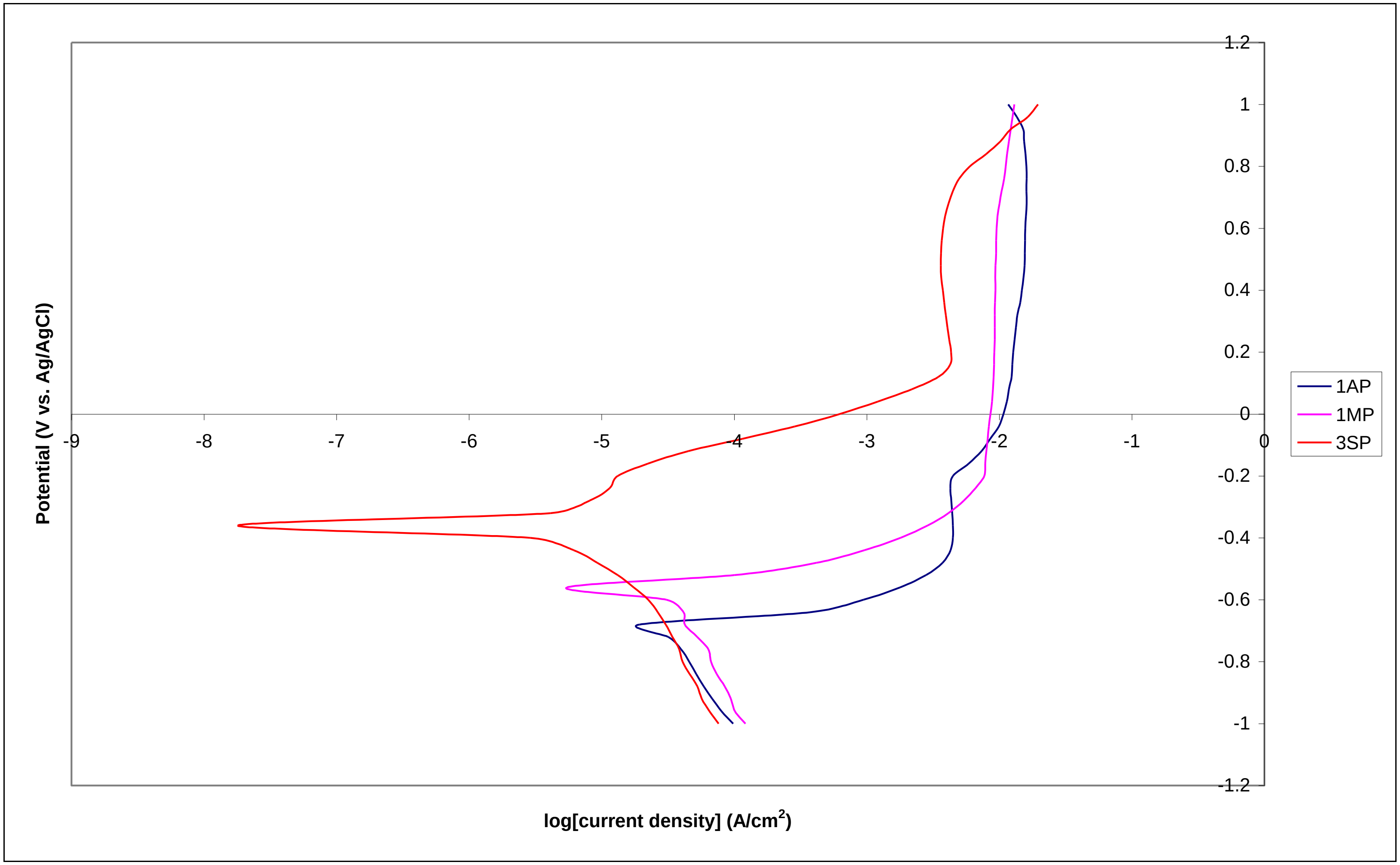

Figure 14: Graph of Plasma coating for the manual experiments

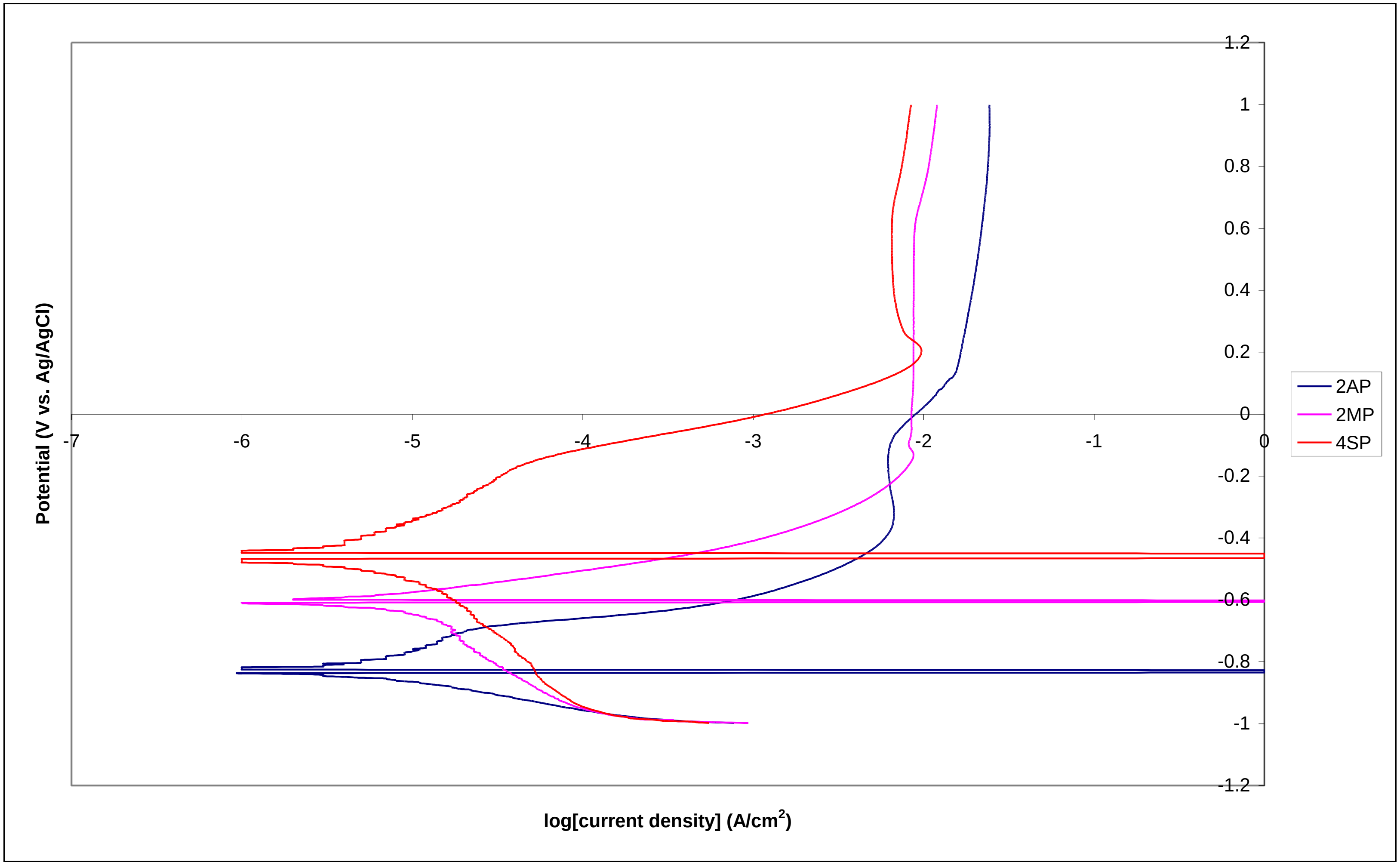

Figure 15: Graph of Plasma coating for the computer controlled experiments.

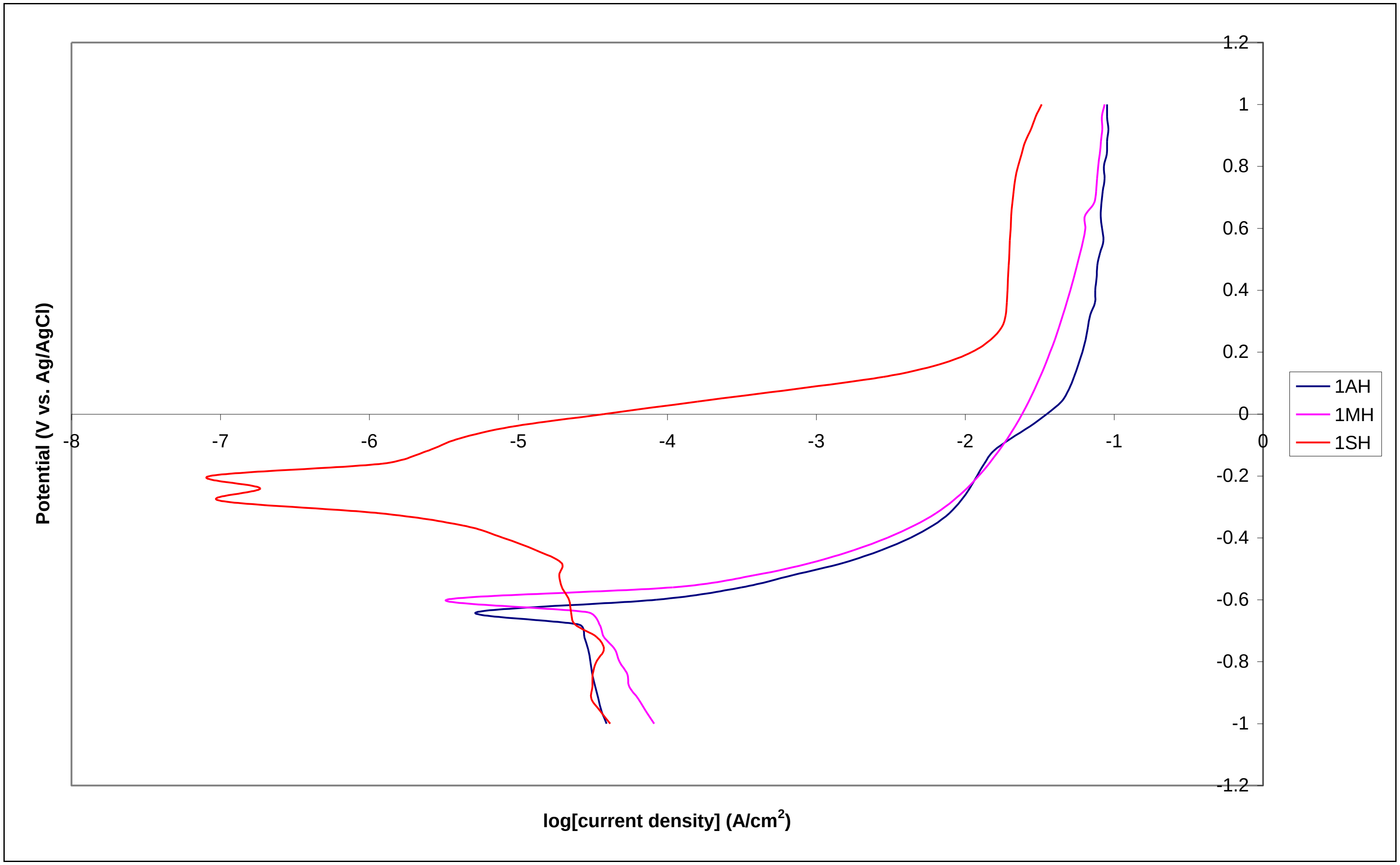

Figure 16: Graph of HVOF coating for the manual experiments.

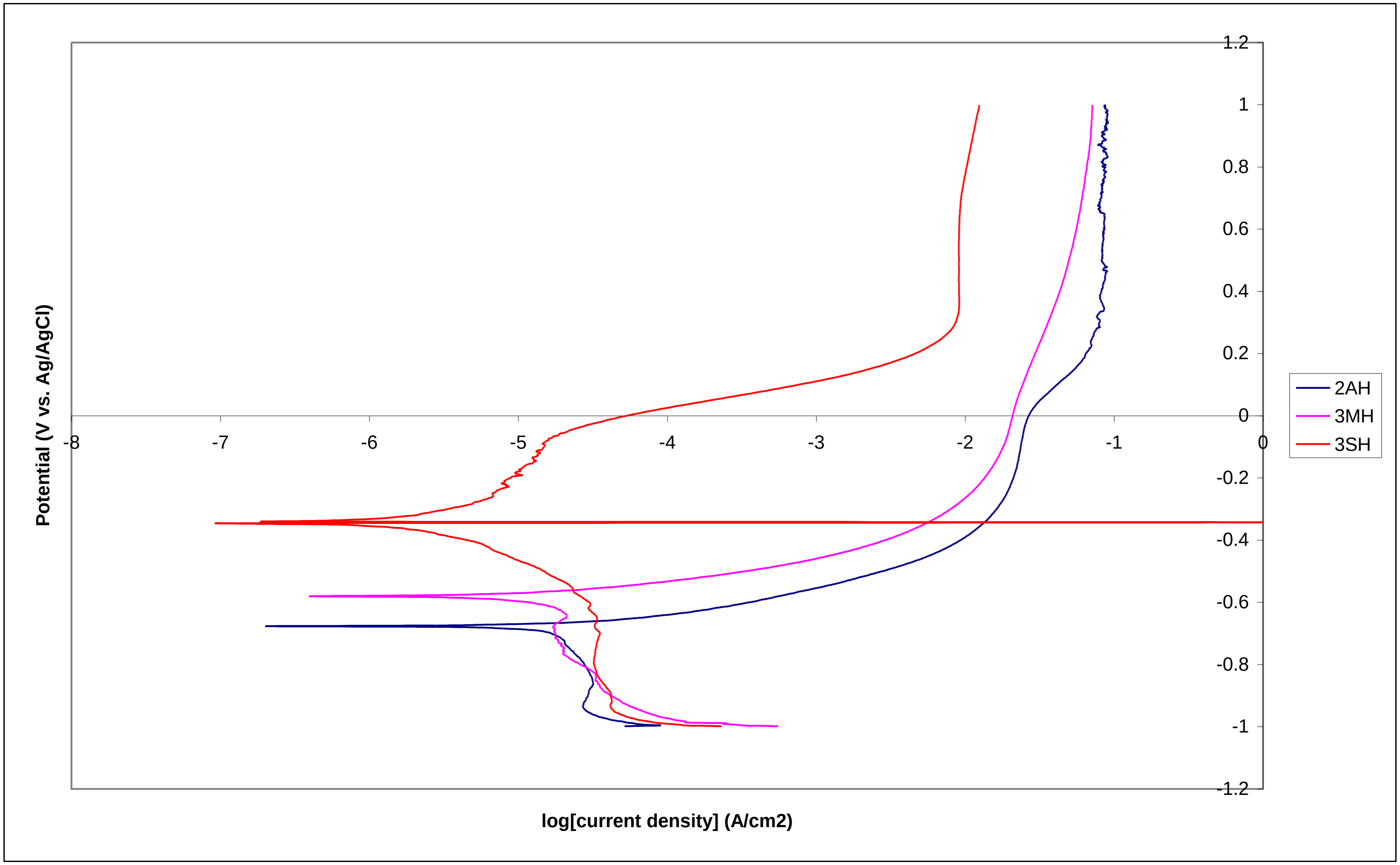

Figure 17: Graph of HVOF coating for the computer controlled experiments.

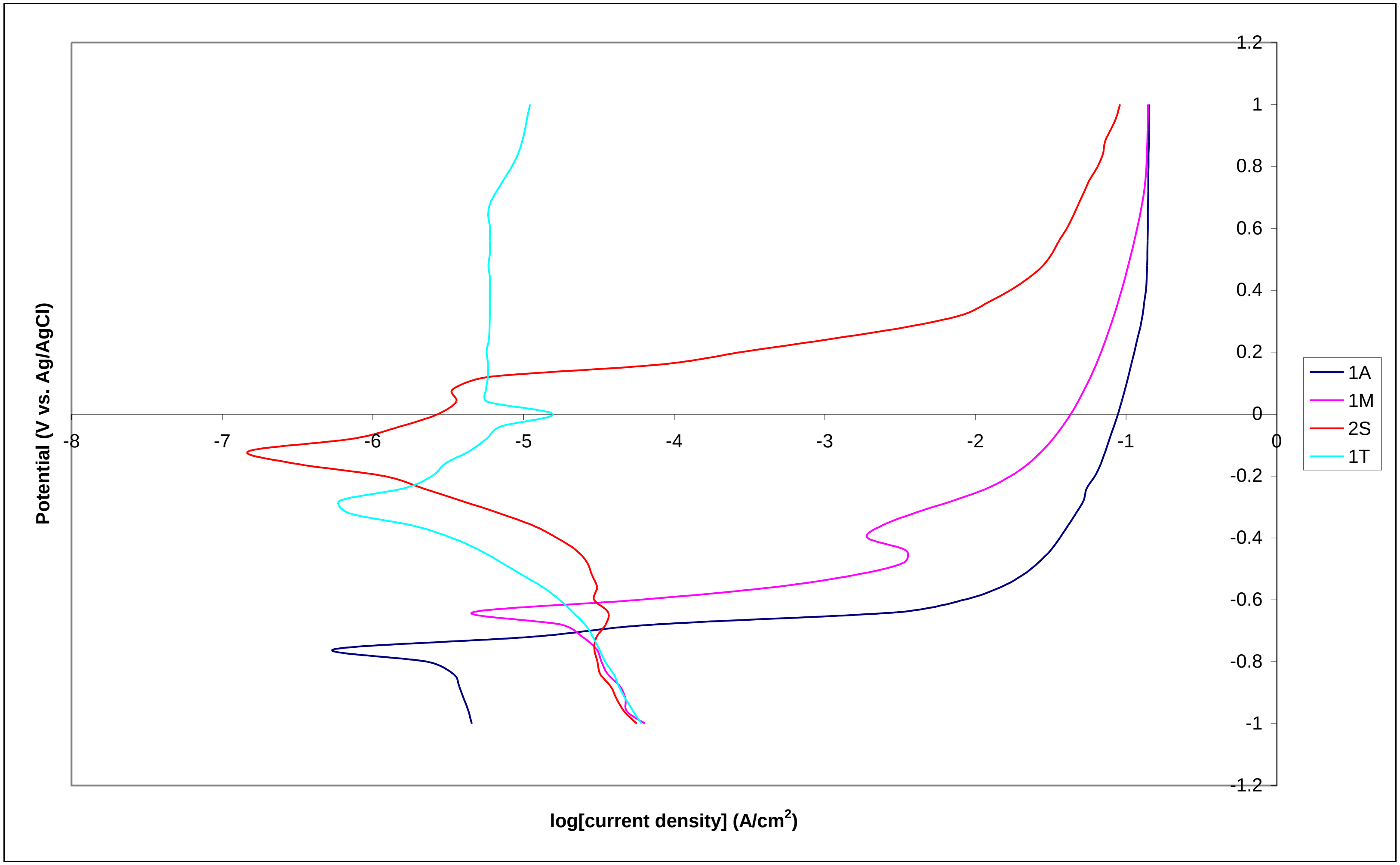

Figure 18: Graph of bare substrates and consolidated Ti powder for the manual experiments.

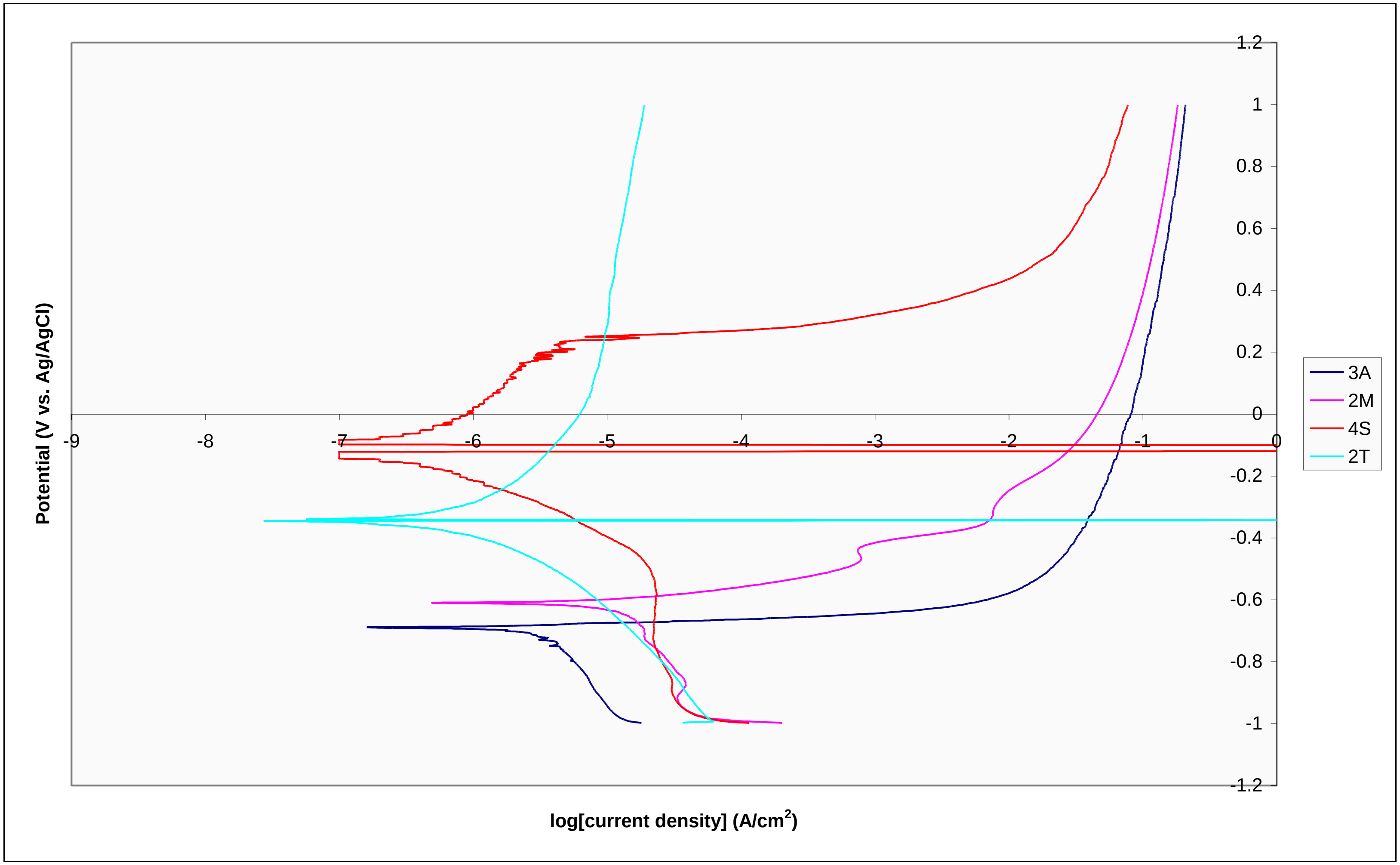

Figure 19: Graph of bare substrates and consolidated Ti powder for the computer controlled experiments.

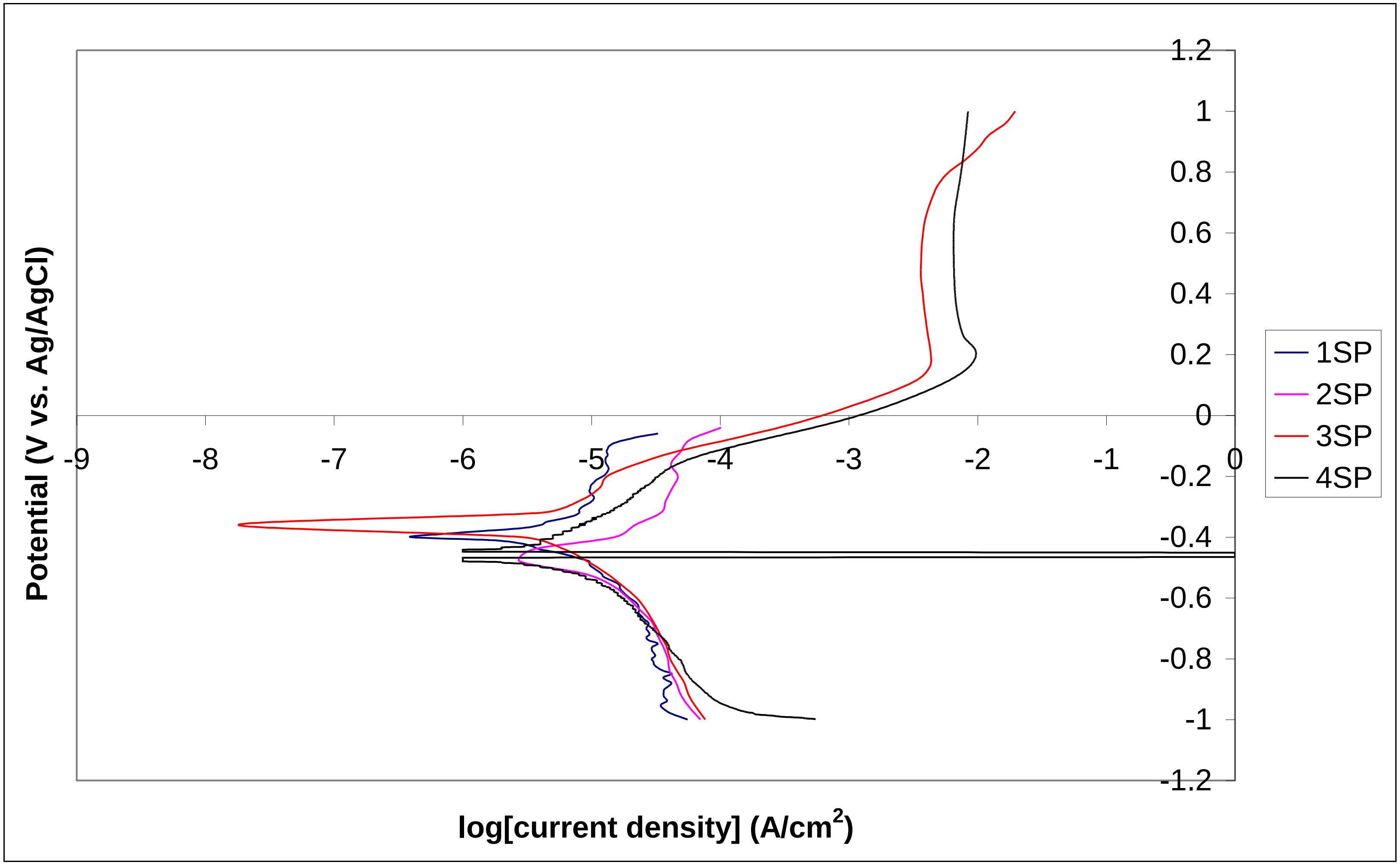

Figure 20: Graph showing the different methods of the experiment.

4.3.1 Missed Designations

There were several sample designations left out of figures 6 – 18. The reasons for leaving them out can be found in table 1.

Designation	Reason it was left out of the graphs
1S	It was believed that the substrate was not the same stainless steel to that which was sprayed. The sample used for 2SP, 3SP and 4SP was the back of a plasma sprayed sample.
3S	Masking was not complete. It was discovered mid experiment.
2SH	When the data was graphed, the current density was abnormally high so the experiment was redone.
2MH	There was gaps in the masking
2A	The sample was repainted with nail polish in light of 3S and 2MH. The sample was not reweighed before the experiment.

Table 1: The reasons for leaving out certain designations.

4.4 SEM Images

Figure 21 and 22 show the SEM images of the untreated and treated powder respectively. It can be seen that the treated powder has less ultra fine particles than the untreated powder. Figure 23 – 31 are the SEM images taken of 1SP, 1AP and 1AH. The 1SP sample was chosen because it was corroded heavily after the experiment so the corrosion mechanism was obvious. The aluminium samples were chosen because aluminium oxide appeared as a darker area on the image so the mechanism for corrosion was obvious. Images with elemental analysis are given to provide a clearer picture of what is going on.

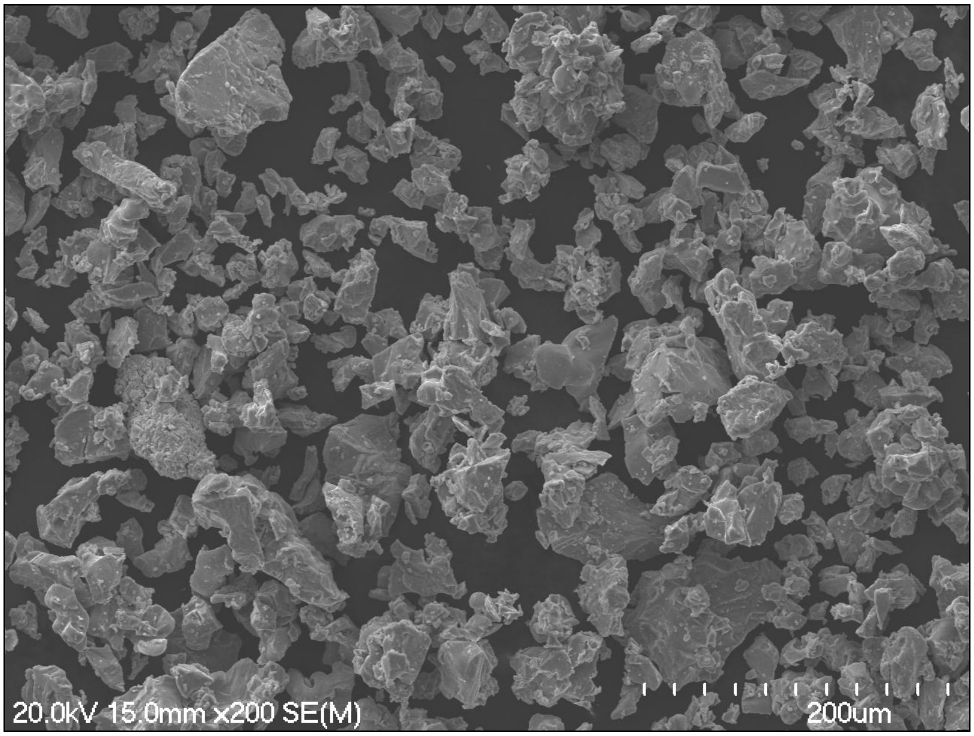

Figure 21: SEM image of untreated powder (x200)

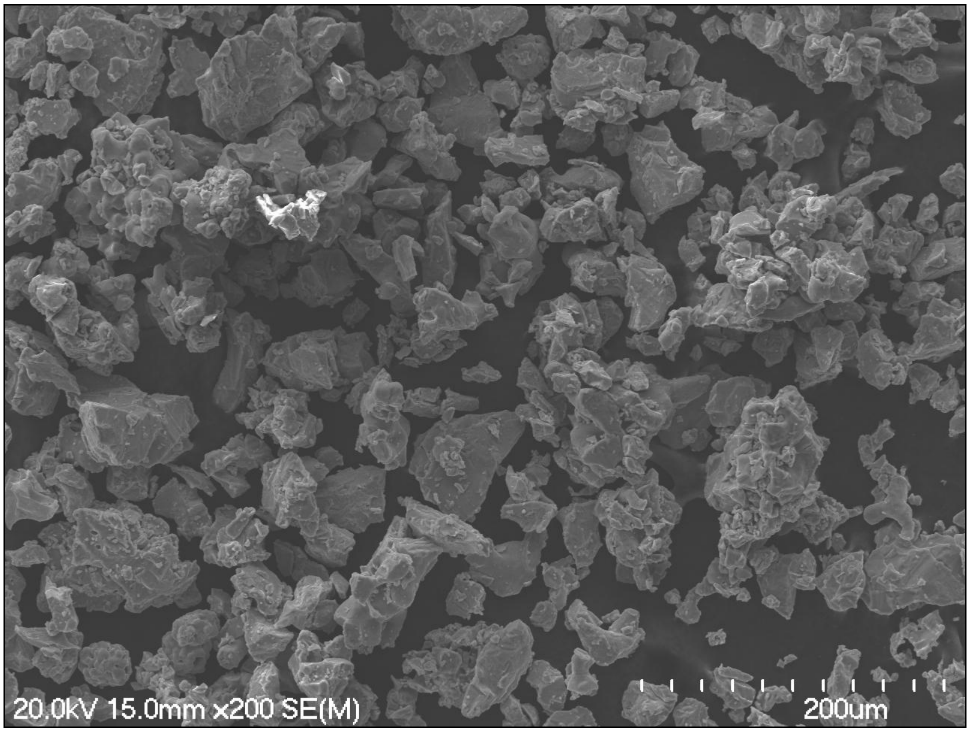

Figure 22: SEM image of powder treated with 3.5% PVA solution (x200).

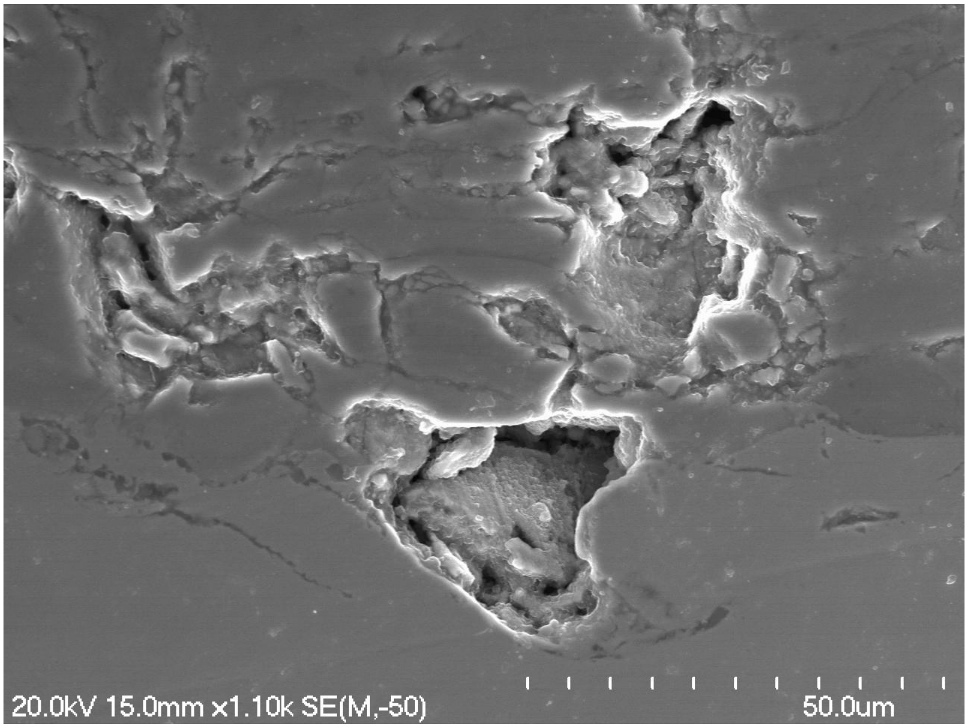

Figure 23: SEM image of the cross-section of 1SP showing a corrosion pit

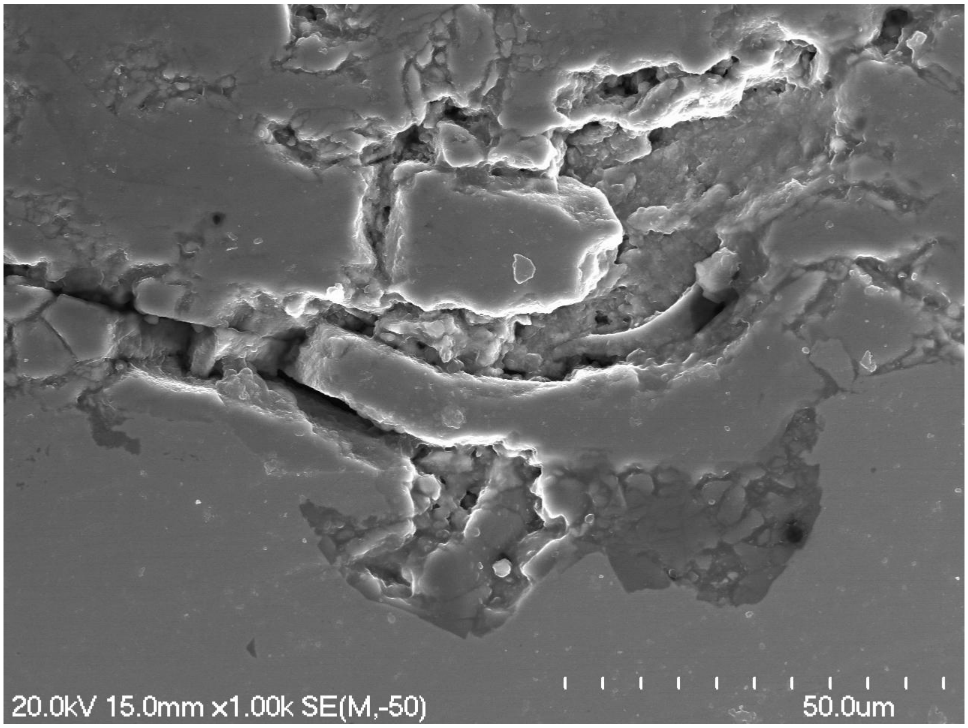

Figure 24: SEM image of the cross-section of 1SP showing another corrosion pit

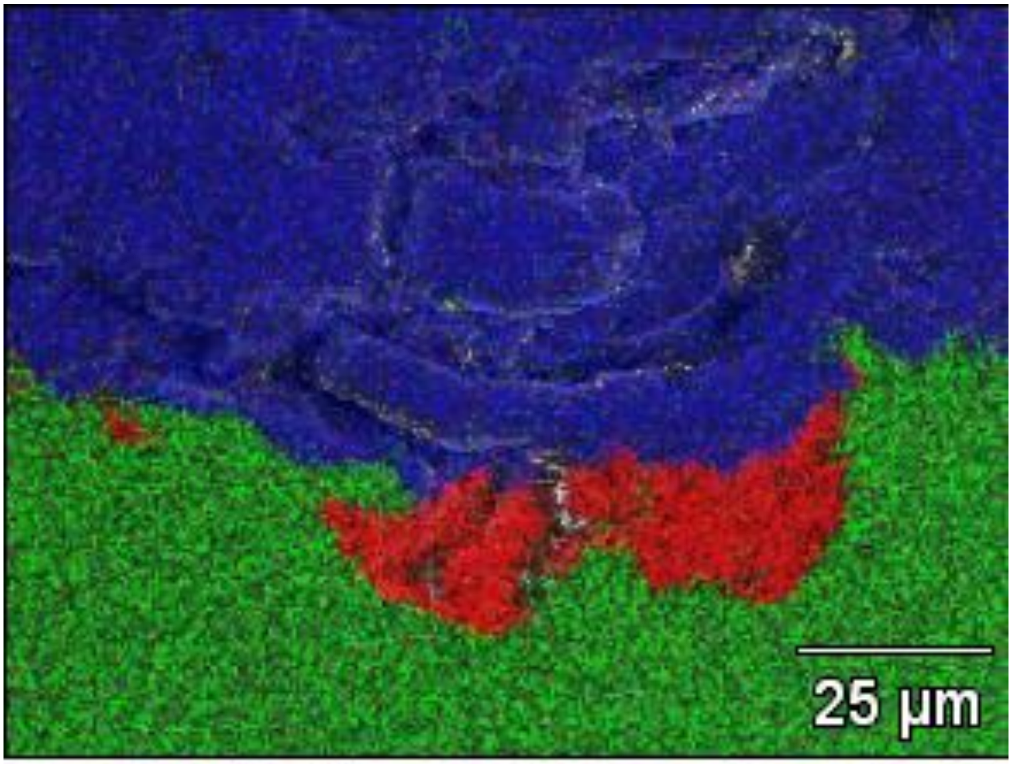

Figure 25: SEM image of the pit in figure 24 with the results of the elemental analysis overlayed. Blue is Ti, green is the stainless steel and red is an Aluminium oxide inclusion.

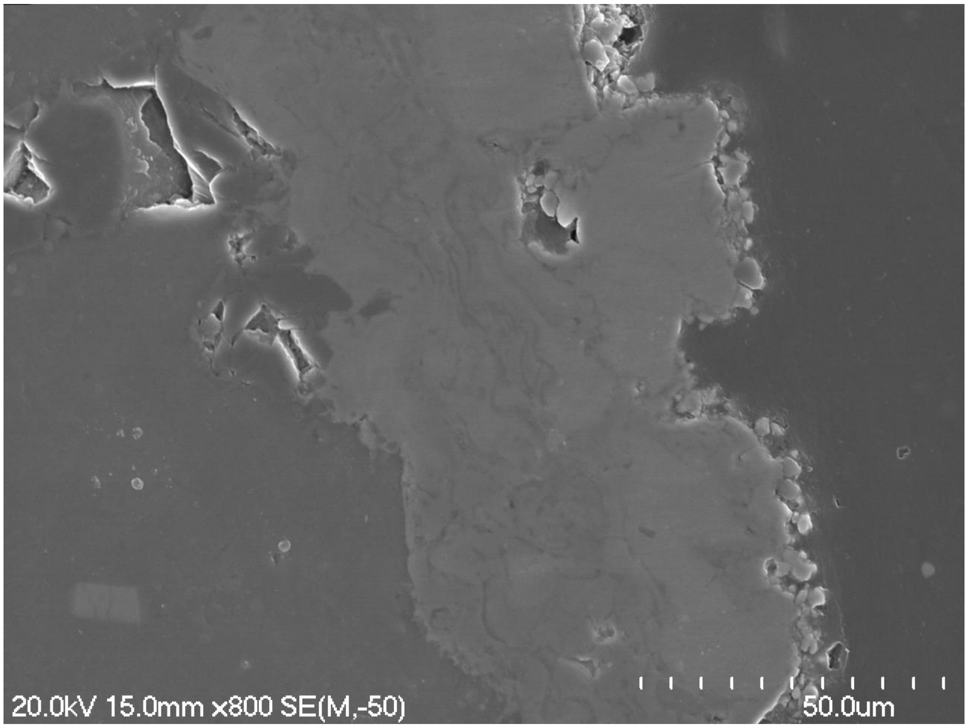

Figure 26: SEM image of a cross-section of 1AP showing some pits.

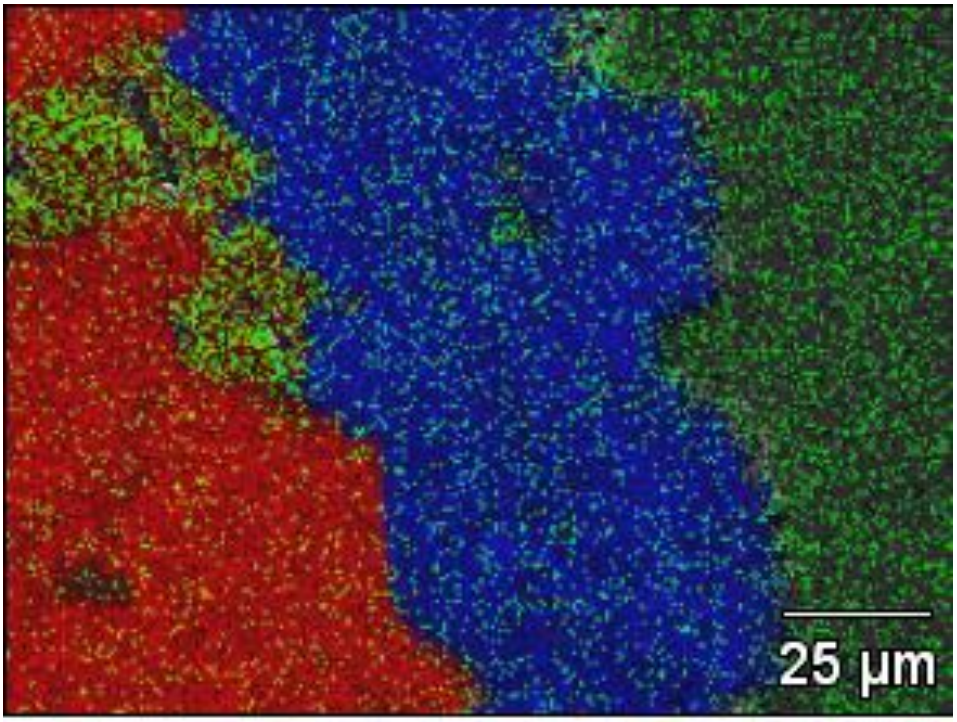

Figure 27: SEM image of the pits in figure 26 with the results of the elemental analysis overlayed. Yellow is Oxygen, blue is Ti and red is Aluminium.

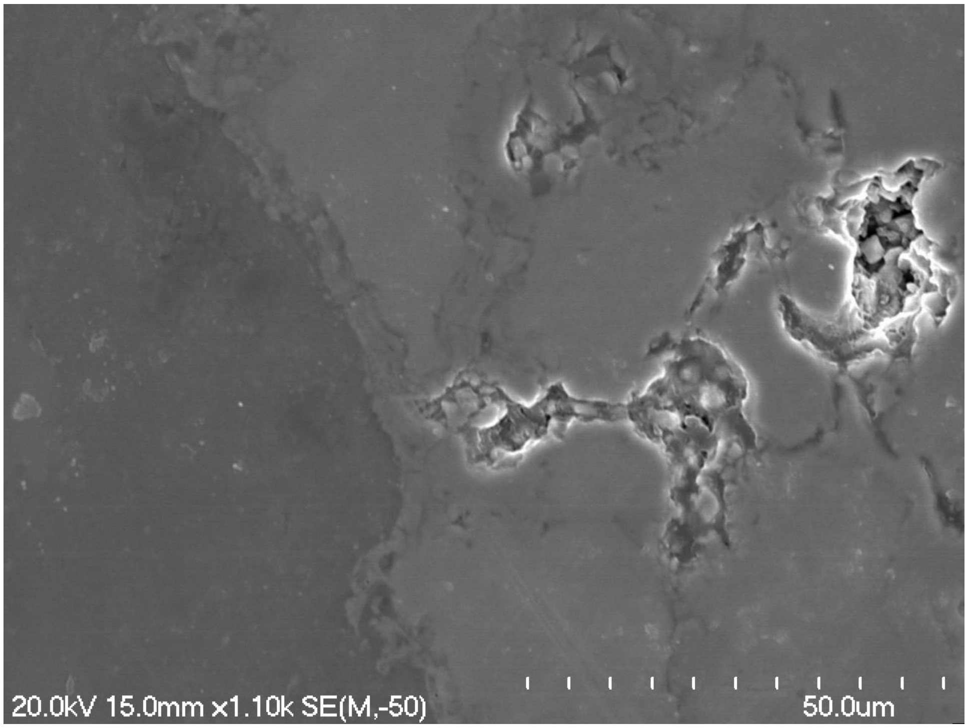

Figure 28: SEM images of cross-section of 1AP showing pits at the end of a pore.

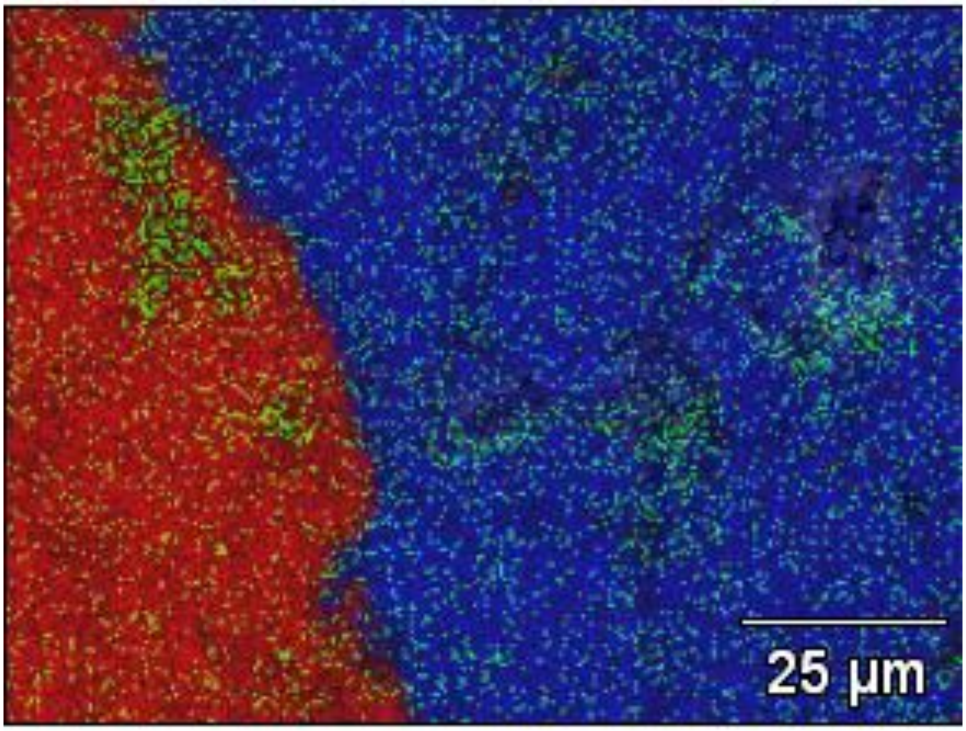

Figure 29: SEM image of the pits in figure 28 with the results of the elemental analysis overlayed. Yellow is oxygen, blue is Ti and red is Aluminium.

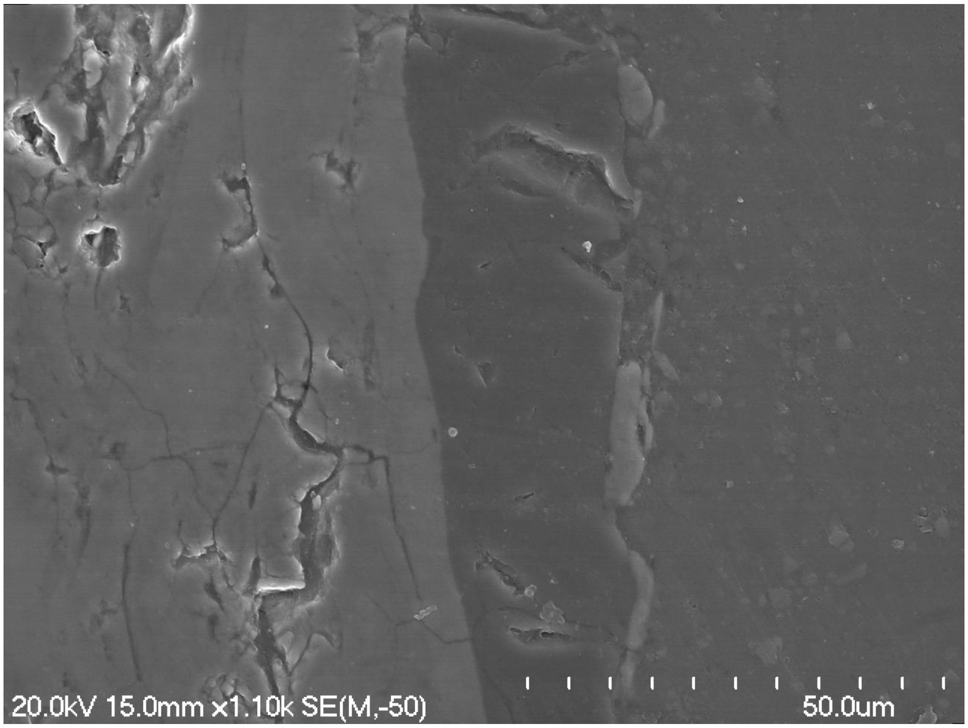

Figure 30: SEM image of cross-section of 1AH showing a band of Aluminium oxide.

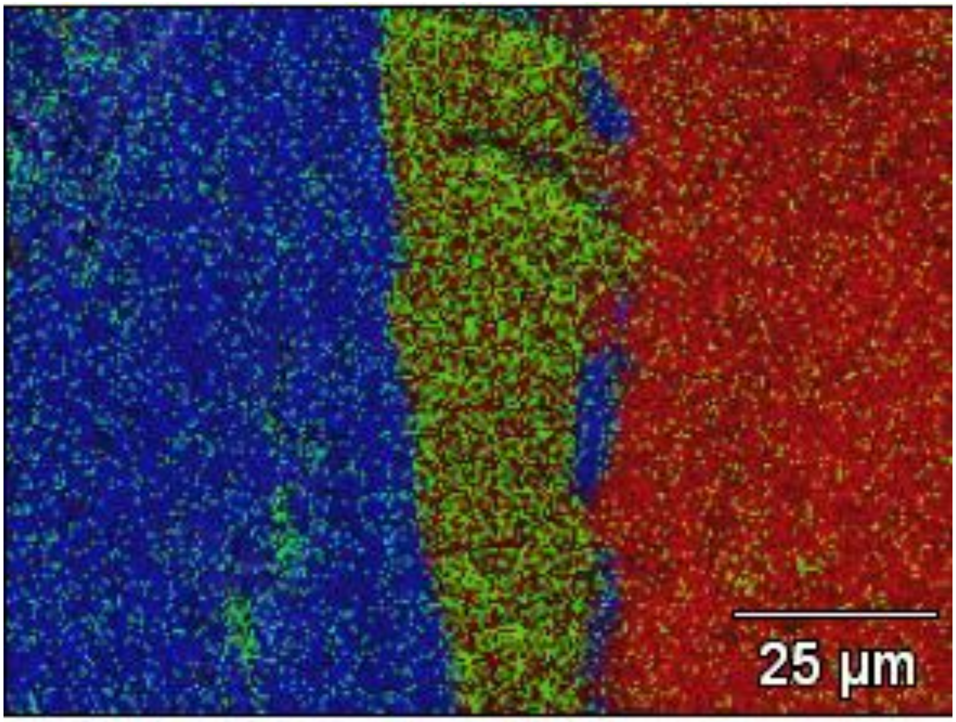

Figure 31: Figure 30 with the results of the elemental analysis overlayed. Yellow is Oxygen, blue is Ti and red is Aluminium.

4.5 XRD results

Figures 32 and 33 show the XRD results for plasma and HVOF coatings respectively. It can be seen that the plasma coating consists entirely of Titanium oxides, where as the HVOF coating predominantly consists of Titanium with some Titanium monoxide.

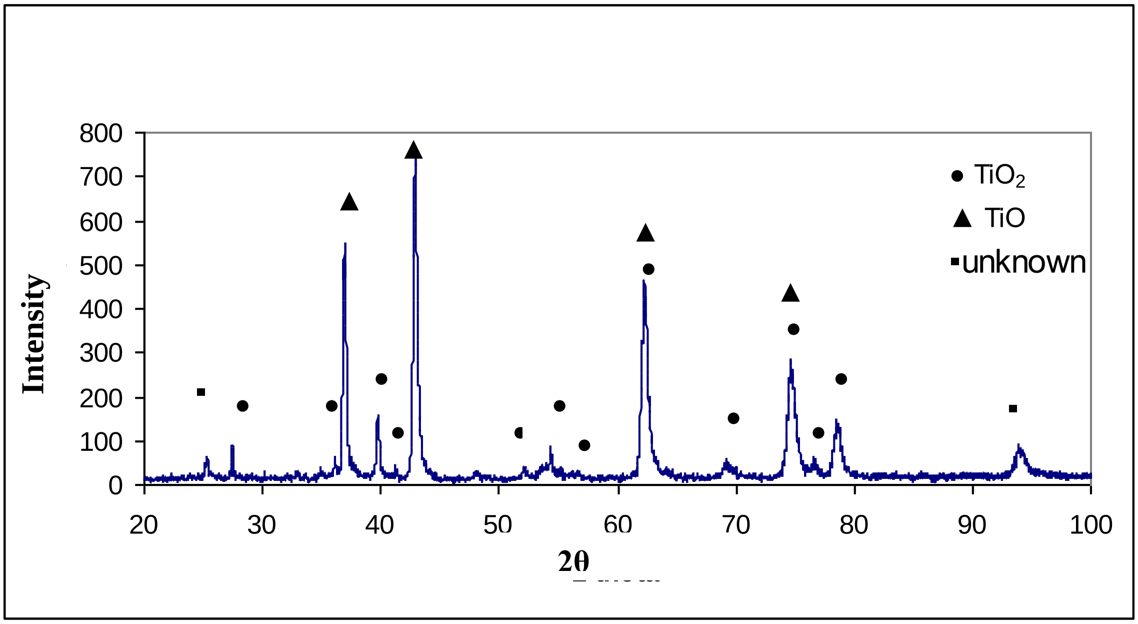

Figure 32: XRD results for Plasma coated stainless steel.

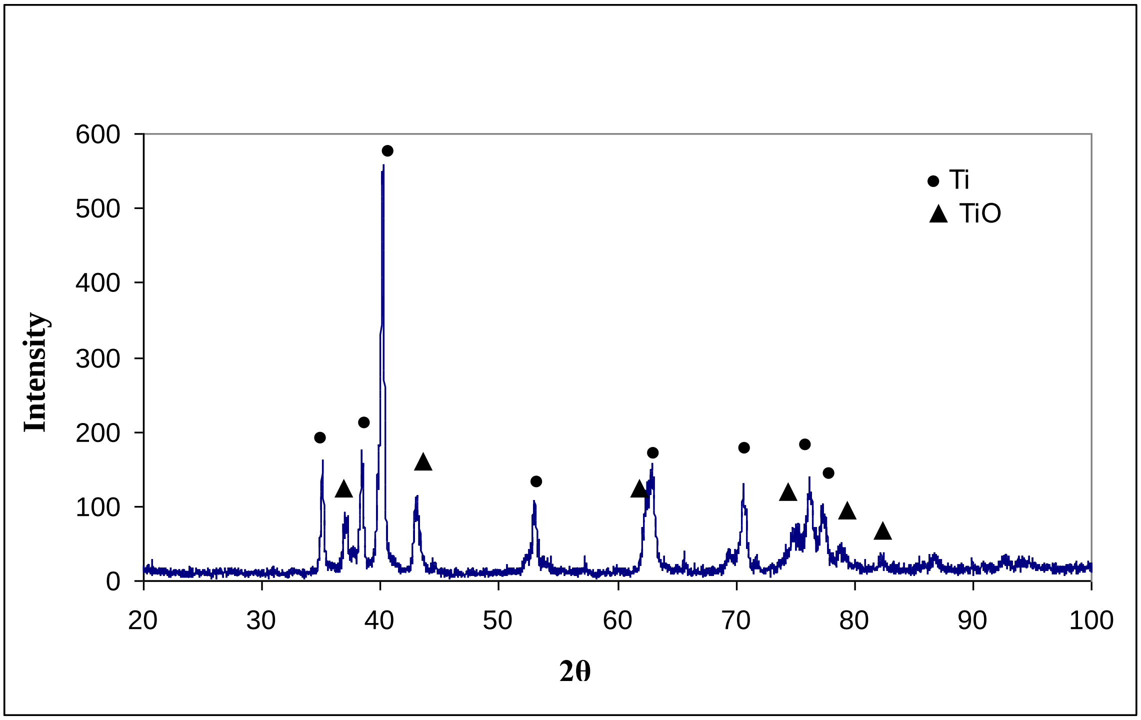

Figure 33: XRD results for HVOF coated stainless steel.

4.6 Density Measurements

Table A5 (appendix A) shows the measurements taken for use in density calculations. The following can be calculated from those measurements:

Plasma Coating:

Thickness of the plasma coating (mm) = 0.321667

Volume of the plasma coating (mm^2) = 3253.571

Mass of the plasma coating (g) = 13.749

Density of plasma coating (g/mm^2) = 0.004226

Density of plasma coating (g/cm^2) = 4.225818

Density of TiO (g/cm^2) [8] = 4.95

Estimate of porosity = 14.63%

HVOF Coating:

Thickness of the HVOF coating (mm) = 0.115

Volume of the HVOF coating (mm^2) = 1155.169

Mass of the HVOF coating (g) = 2.322

Density of HVOF coating (g/mm^2) = 0.00201

Density of HVOF coating (g/cm^2) = 2.010096

Density of Ti (g/cm^2) [8] = 4.5

Estimate of porosity = 55.33%

The estimate of porosity for the two coatings was found by comparing the density of the coatings to the density of the material which is most prominent in the coating (give by figures 28 and 29)

4.7 pH Measurements

The following measurements were taken with a Radiometer MeterLab PHM240 pH meter.

Distilled water used to create electrolyte = 7.27

NaCl 3.5% solution by weight = 6.27

It can be seen that the addition of 3.5% NaCl lowers the pH by 1 (more acidic)

4.8 Pourbaix Diagrams

Figure 34 to 36 show the Pourbaix diagrams in chloride solution for Titanium, Iron, and Stainless steel (Fe-Cr-Cl-H_2O) respectively. Figure 37 shows the Pourbaix diagram for Aluminium in aerobic seawater. The diagrams for Iron, Stainless steel and Aluminium are at 25°C, which associates to room temperature (which the experiments were carried out at). The diagram for Titanium however, is at 75°C, but upon comparison with the Pourbaix diagram for the Ti-H_2O system [9] it appears that figure 34 is a reasonable approximation to the Ti-Cl-H_2O system for 25°C. Iron was used to approximate mild steel. Inspection of the Pourbaix diagrams between -1 and 1V for a pH of around 6 (as per section 4.7), reveals the following:

- Titanium should passivate from about -0.3 to 1V.

- Mild steel should passivate from about 0.2 to 0.4V if at all.

- Stainless steel should passivate from about -0.6 to 0.5V.

- Aluminium should passivate from about -1 to 1V

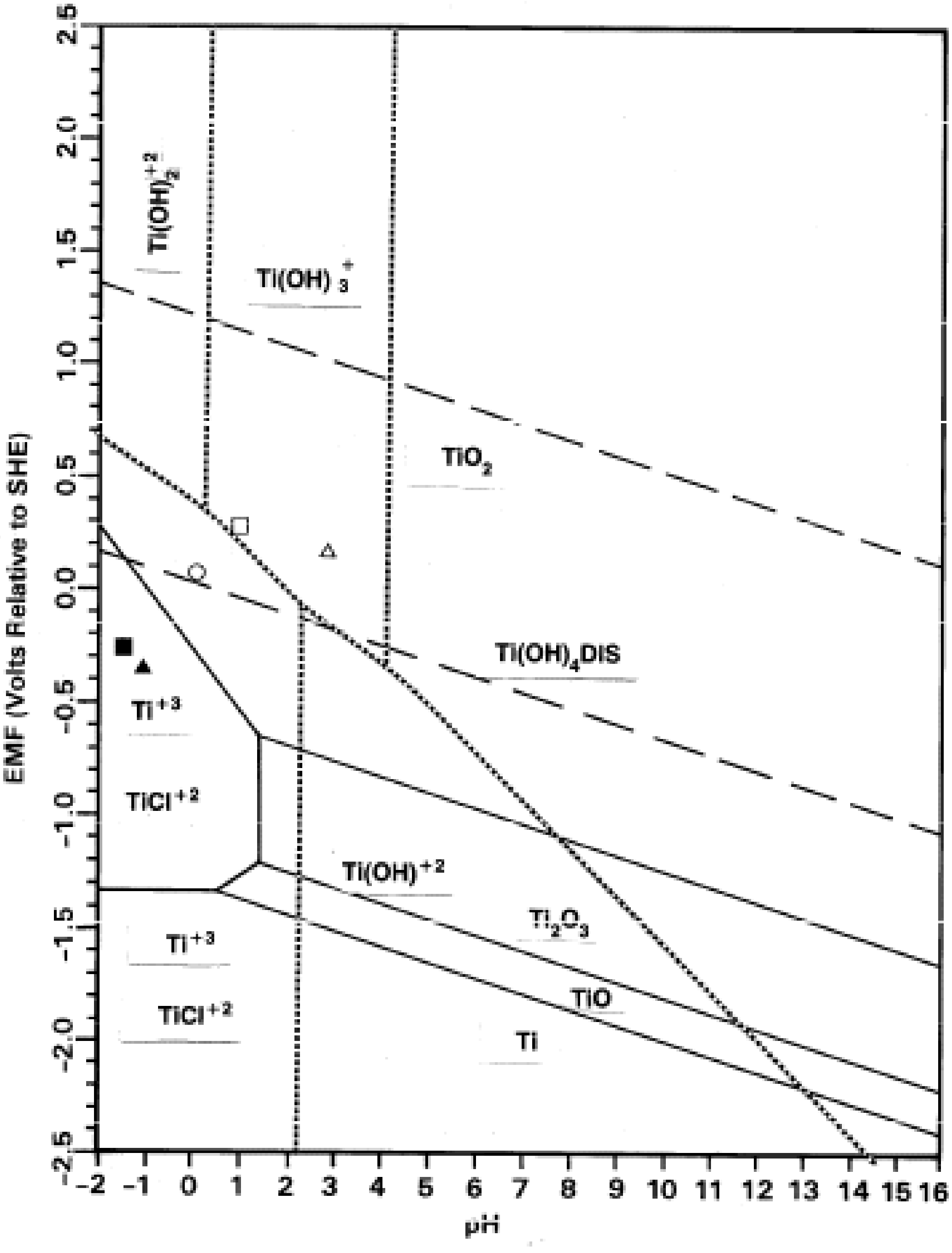

Figure 34: Potential - pH equilibrium diagram for the Ti-Cl-H_2O system at 75°C [10]

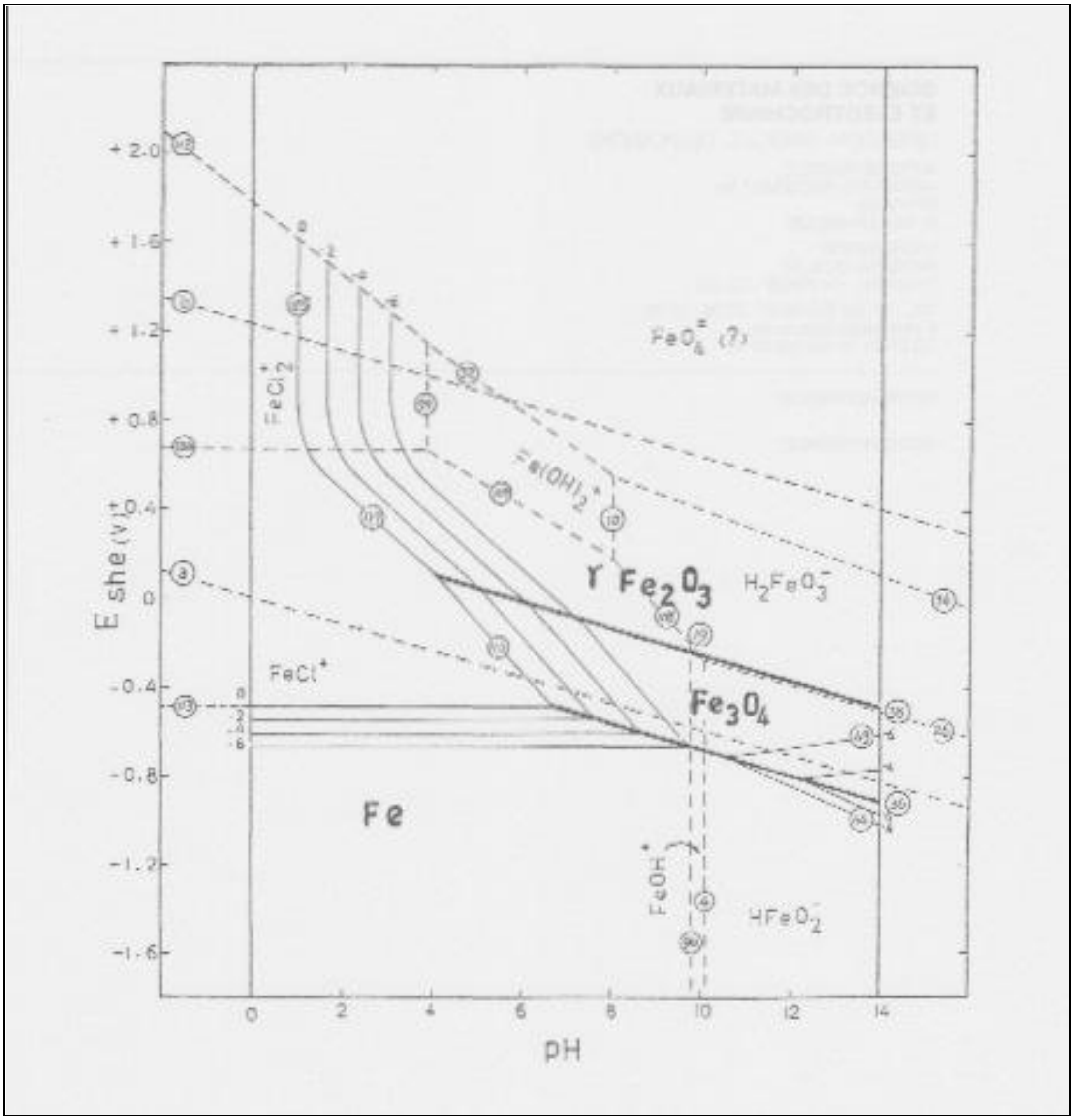

Figure 35: Potential - pH equilibrium diagram for the Fe-Cl-H_2O system at 25°C [11]

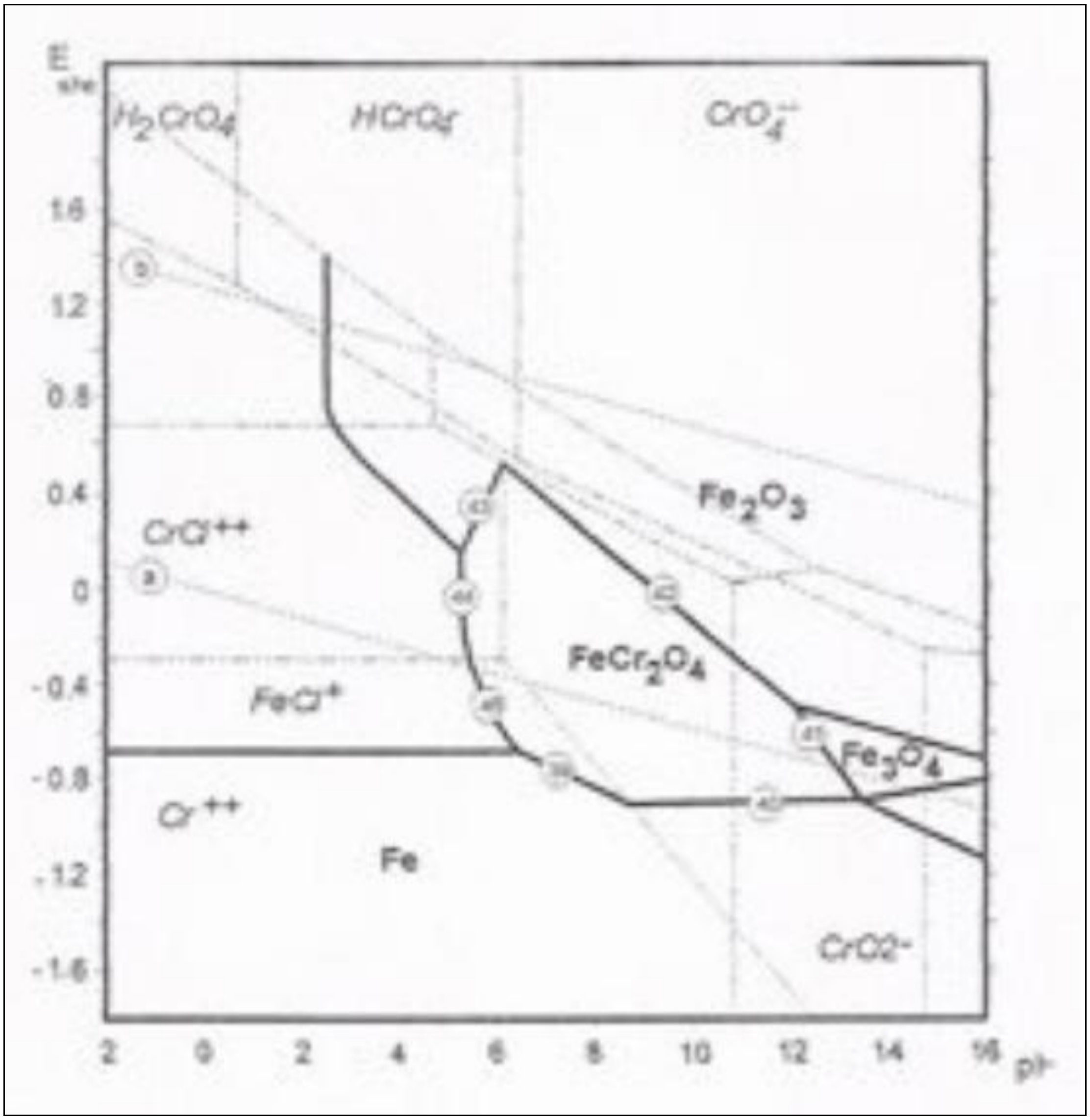

Figure 36: Potential - pH equilibrium diagram for the Fe-Cr-Cl-H_2O system at 25°C [12]

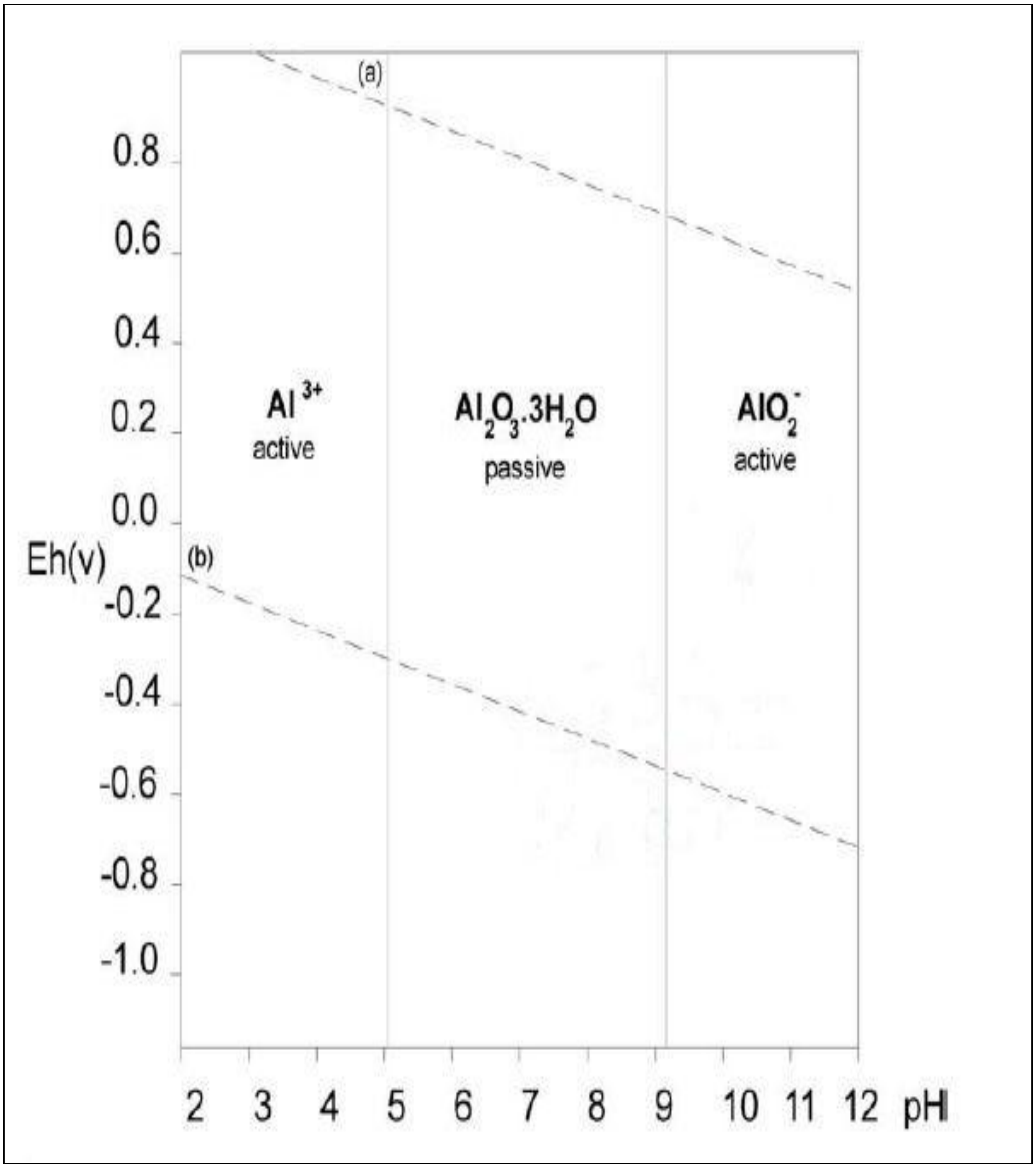

Figure 37: Potential - pH equilibrium diagram for Al in aerobic seawater at 25°C (modified from [13])

5.0 Discussion

It can be seen in figure 1 that the untreated powder and the powder treated with 3% PVA solution are different. The treated powder seems to have more uniform particles than the untreated powder. The treated powder has a pile indicative of a well flowing powder; which is due to the more uniform particle size. Figures 21 and 22 also support this. The treated powder has fewer ultra fine articles than the untreated powder. The ultra fine particles in the treated powder are combined with other particles by the PVA solution to create more uniform particle size. These ultra fine particles hinder the flowability of the untreated powder.

From the graphs of substrates (figures 8 – 13) it can be seen that there is one thing common to all graphs; plasma coatings have better corrosion behaviour than HVOF. This is especially true in the later section of the graphs. The reason that the plasma coatings perform better than HVOF is a function of multiple factors. The main reason is that the plasma coating has far less porosity than HVOF (plasma has 14.63% and HVOF has 55.33%). This gives the electrolyte less passageways to the substrate through the coating and also allows the coating to passivate more effectively. The difference in passivation can best be seen in the mild steel, with the plasma coating passivating fully, while the HVOF either not passivating or not passivating very well.

The better corrosion resistance of the coated samples is evidenced in the graph of metal gain/loss (figure 7). In general the metal loss for the substrates is more than that of the HVOF (if the designations that were excluded from the polarisation curves for the reasons given in section 4.3.1 are excluded). The samples coated by plasma spraying have less metal loss than HVOF and most of the plasma sprayed samples had a metal gain as a result of the experiments. The less the samples corrode, the less the metal loss and when the weight of the passive film exceeds that of the metal lost as corrosion product; a metal gain results. The plasma coating method provides the greatest improvement in metal loss and thus provides the greatest improvement in corrosion resistance.

This difference in porosity is a function of both the thickness of the plasma coating and the extreme temperatures at which the plasma spraying system operates. Both the coatings had five passes in spraying, so the difference is due to the way that the two spray methods deposit. The plasma spray method shoots molten Titanium, so with each successive pass; the molten Titanium fills the pores of the previous pass. The HVOF spray method relies on velocity for deposition, so a lot of the Titanium bounces off the surface (which is why the coating weighs less than plasma) so the pores are not filled to the same extent. Another factor that contributes to the difference between plasma and HVOF is the composition of the coating. From figures 32 and 33 it can be seen that the most prominent species in HVOF is Titanium and in plasma is Titanium oxides. The key to Titanium’s corrosion resistance is the oxide layer; so based on this the plasma coatings should have higher corrosion resistance.

All of the coated samples exhibited the same kind of curve: They pitted before they passivated. The pitting is where the graph has a large increase in current density for a small increase in potential. This happens because of the surface roughness of the coatings. The roughness of the surface creates high energy sites for corrosion to take place; so corrosion takes place in a localised way. This is in line with literature as Hong-Ren et al. found that the unpolished as sprayed coatings exhibit lower corrosion resistance due to the surface activity [6]. The pores in the coating also provide pathways to the substrate. The end of the pore at the substrate is an area of low oxygen, while the end at the surface has high oxygen. This creates a corrosion cell and highly concentrated corrosion takes place. Once the rate of passivation exceeds the rate of pitting; the rate of current density increase slows down and then the graph indicates passivation (little or no increase in current density for a large change in potential).

The mechanism of corrosion of pitting at the end of pores is further evidenced by the SEM images (figure 23 -31). The pits in 1SP were obvious due to the fact that the working electrode was excessively corroded after the completion of the experiment. The Aluminium images were chosen because Aluminium oxide has a darker colour in the SEM image than Aluminium. All the aspects of the corrosion story can be seen in the Aluminium images. The SEM images of 1AP show evidence of pitting at the end of pores (especially figure 28). The cross-section in figure 26 does not slice perfectly through the pores, but there is still evidence of a pore above the pit.

In the images of 1AH (figures 30 and 31), the difference between plasma and HVOF coatings can be seen. The 1AH images show that pitting has occurred more excessively and has caused a continuous section of Aluminium oxide to form. There were several sections like that along the area exposed to corrosion, showing that corrosion of the substrate occurred to a larger extent than the plasma coating. The difference in porosity is also evident in the images of 1AP and 1AH. The HVOF coating is clearly more porous, but also has gaps throughout the coating. The gaps may be between the splatters of the coating. The plasma coating has a more solid structure due to the high temperatures; allowing the splatters to melt together.

A comparison of the polarisation curves for the substrates for mild steel and Aluminium (figures 10 & 11 and 12 & 13 respectively) shows that both coating types improve the corrosion resistance of the substrate. This is especially true for Aluminium, as the coatings add a second passivation at a lower potential. The second passivation can best be seen in the computer controlled experiments and is more pronounced for the plasma coating method. A comparison of the stainless steel curves (figures 8 and 9) does not give such a clear indication of an improvement in corrosion resistance. In the curve for the substrate, passivation occurs early on and can be seen best in the computer controlled experiment from approximately -0.2V to 0.5V. In the curves for the coatings, passivation occurs later; from approximately 0.2V to 0.8V. The early passivation for the substrate is not very stable; this is indicated by the slanted nature of the curve. It is caused by passivation occurring at the same time as pitting. The pitting rate is greater than the rate of formation of the passive film, so the graph has a gradient at that point. The passivation for the coating curves happens over a similar length of voltage, but the passive film is much more stable (evidenced by little or no change in current density for a large change in potential). Because the passive film is more stable in chloride solution it can be concluded that the coatings do provide better corrosion resistance for stainless steel. Just like the case for mild steel and Aluminium, the plasma coating method provides the best corrosion resistance.

When the graph of the bare substrates (figures 18 and 19) is compared to the graphs of Plasma (figures 14 and 15) and HVOF (figures 16 and 17) coatings, it becomes apparent that the substrates play a large role in the features of the graph. If the graphs are compared in the positive potentials; the spacing between the graphs is similar. This is due to the porous nature of the coatings. When the electrolyte travels through the pores and contacts the substrate; the substrate reacts and the curve follows the substrates to a certain extent. The polarisation curves for the plasma coatings produced under computer control (figure 15) follows a slightly different pattern. Those for plasma coated mild steel are similar in terms of placement, but the curves for 2AP and 4SP have higher current densities for passivation than that of their manual counterparts (1AP and 3SP respectively). Slight differences from place to place over the surface of the substrates can explain this. Although all of the coated samples have some aspects of their polarisation curves in common with those of their corresponding substrates, it can be seen that the plasma coated samples have less in common with the curves of the substrate than the HVOF coated samples. This can again be explained by the amount of porosity and can be best explained with reference to the mild steel sample. The HVOF curve follows the substrate curve closely, but the plasma passivates instead of following the curve all the way. Mild steel shows the best improvement from plasma spraying, as the bare substrate doesn’t passivate.

Figure 20 shows the polarisation curves for stainless steel after plasma spraying and obtained using different experimental methods. In the manual experiments it can be seen that when the step size is increased from 10mV per step (1SP) to 40mV per step (2SP), the current densities of the curves increase. When the time after each step was changed from unlimited (2SP) to one minute (3SP), the current density increased as well. This is consistent with literature that says that longer periods at each step result in lower currents [1]. This pattern is continued when the scan rate is increased to 1mV/sec (4SP) in the computer controlled experiments (with an associated increase in current densities).

Before a discussion of the Pourbaix diagrams is carried out it is important to note that the diagrams are based on thermodynamics and reveal nothing about the rates of corrosion or passivation [1]. The discussion refers to the diagrams in section 4.8 between -1 and 1V for a pH of 6. Also, the data from experiments is from the computer driven experiments (figures 9, 11, 13, and 19).

The polarisation curve for consolidated Titanium powder passivates between about 0 to 1V. This follows the Pourbaix diagram reasonably closely. Although the Pourbaix diagram has passivation from about -0.3 to 1V, the rate of passivation may be low from -0.3 to 0V and thus is not fast enough to prevent further corrosion. The polarisation curve for mild steel shows no passivation. The rate of corrosion slows down in the range for passivation predicted by the Pourbaix diagram, but the passivation rate is probably not fast enough to fully compensate for the corrosion rate and achieve full passivation. The polarisation curve for stainless steel shows an unstable passivation from about -0.1 to 0.3V. The unstable passivation may be caused by the fact that a pH of 6 lies closely to the boundary between passivity and corrosion on the Pourbaix diagram, so both passivation and corrosion are occurring. The polarisation curve for Aluminium does not fully passivate, but the rate of corrosion slows down between about -0.7 to 1V. The difference between the Pourbaix diagram and the polarisation curve can be explained by several things. The Pourbaix diagram was for seawater not a chloride solution. Also, the Pourbaix diagram was used in reference to a decommissioned naval vessel. Finally, the rate of passivation layer formation may be insufficient to suppress the corrosion rate completely.

If the polarisation curves for the plasma coatings are compared to the Pourbaix diagrams the effect of the best coating type for the experiments becomes apparent. The polarisation curve for mild steel coated using plasma spraying shows that passivation occurs from about -0.1 to 0.6V. This is a vast improvement thermodynamically in that the range of passivation increases by over three times. The stainless steel has an improvement thermodynamically as well. Instead of only passivating once, it passivates from about -0.4 to -0.3 and between 0.2 and 1. The polarisation curve for Aluminium coated using plasma spraying shows a reduction in rate for the same range of voltage as the substrate polarisation curve, which means that thermodynamically the Aluminium stays the same when coated using plasma spraying. The rate of passivation however, is greatly improved. The plasma coated Aluminium properly passivates from -0.4 to 1V which means the rate of passivation is sufficient to suppress the corrosion rate.

6.0 Conclusions

From the discussion the following can be concluded:

- The plasma coating provides the best corrosion resistance due to the fact that it had less porosity than HVOF and that it is made up of Titanium oxides.

- The corrosion mechanism for the coatings is pitting of the substrates at the end of pores. The extent of this is far greater for the HVOF than the plasma coating.

- Features found in the polarisation curves for the substrates are present in the curves for coatings. This is more evident in the HVOF polarisation curves.

- Mild steel benefited the most from the Titanium coatings compared to the substrate (more so for the plasma coating).

- The plasma coating improves the substrate based on corrosion rate and thermodynamics, except for Aluminium which remains the same thermodynamically.

7.0 Recommendations for Future Work

Experiments should take place to compare Plasma and HVOF with other spray methods such as cold spraying. Further investigation into the other qualities of the coatings should be done; such as whether the oxide nature of the plasma spray method affects the brittleness and adhesion of the coating. Investigation into methods of filling the pores of the coatings is also recommended. Methods may include adding Chromium to the powder mix [3], adding another coating, and remelting the coating after spraying.

8.0 References

1. Jones, D.A., *Principles and Prevention of Corrosion*. 1996, New Jersey: Prentice-Hall.
2. Perillo, P.M., *Corrosion behavior of coatings of titanium nitride and titanium-titanium nitride on steel substrates.* Corrosion, 2006. **62**(2): p. 182-185.
3. Mao, Z., et al., *The effect of powder preparation method on the corrosion and mechanical properties of TiN-based coatings by reactive plasma spraying.* Applied Surface Science, 2009. **255**(6): p. 3784-3788.
4. Baba, K. and R. Hatada, *Corrosion-resistant titanium nitride coatings formed on stainless steel by ion-beam-assisted deposition.* Surface and Coatings Technology, 1994. **66**(1 -3 pt 2): p. 368-372.
5. Wu, G., et al., *Improving corrosion resistance of titanium-coated magnesium alloy by modifying surface characteristics of magnesium alloy prior to titanium coating deposition.* Scripta Materialia, 2009. **61**(3): p. 269-272.
6. Hong-Ren, W., et al., *Corrosion behavior of cold sprayed titanium protective coating on 1Cr13 substrate in seawater.* Surface and Coatings Technology, 2007. **201**(9-11): p. 5203-6.
7. Scholz, F., ed. *Electroanalytical methods :guide to experiments and applications*. 2002, Springer: Berlin. 331.
8. *Chemical Book*. 2008 [cited 14 February 2010]; Available from: http://www.chemicalbook.com/.
9. Donachie, M.J., *Titanium: A Technical Guide*. 2nd ed. 2000, Ohio: ASM International.
10. Silverman, D.C. *TUTORIAL ON THERMEXPERT™ Potential-pH (Pourbaix or EMF-pH) Diagram Generator*. [cited 3 March 2010]; Available from: http://www.argentumsolutions.com/tutorials/thermexpert_tutorialpg5.html.
11. YANG, X.-Z. *Potential-pH Equilibrium Diagrams for the Fe - Cl - H2O System at Temperatures up to 300°C*. [cited 3 March 2010]; Available from: http://server2.publiset.be/publiset/cebelcor/publications.lasso?Id=156.
12. L.X.Yang, X.Z.Yang, and A.Pourbaix. *Potential-pH diagrams relevant to 13Cr stainless steels in chloride and sulfide containing solutions*. 2001 [cited 3 March 2010]; Available from: http://server2.publiset.be/publiset/cebelcor/publications.lasso?Id=86.
13. I. MacLeoda, P.M., V.Richardsa, N. Westc. *Corrosion monitoring and the environmental impact of decommissioned naval vessels as artificial reefs*. 2004 [cited 11 March 2010]; Available from: http://www.nma.gov.au/shared/libraries/attachments/publications/metal_04_proceedings/section_1_preventive_conservation/files/7821/NMA_metals_s1_p5_corrosion_monitoring.pdf.

Appendix A: Tables

Parameter	**Plasma**	**HVOF**
H wheel for powder flow	15 RPM	91 RPM
Air vibrator	8 psi	60 psi
O_2 regulator pressure		100 psi
H_2 regulator pressure	85 psi	
N_2 regulator pressure	100 psi	100 psi
Air regulator pressure	700 kpa	700 kpa
Propane regulator pressure		60 psi
O_2 flow rate		90
H_2 flow rate	10	
N_2 flow rate	75	
Air flow rate	40	45
Propane flow rate		50
Spray distance	3.5 - 4 inches	6.5 - 7 inches
Passes	5	5

Table A1: Parameters of spraying equipment.

Designation	**Substrate**	**Coating**	**Masking**	**Method**	**Step Size / Scan Rate**
1SP	Stainless steel	Plasma	Wax	Manual	10mV/step
2SP	Stainless steel	Plasma	Wax	Manual	40mV/step
1T	Titanium	None	Wax	Manual	40mV/step
3SP	Stainless steel	Plasma	Nail polish	Manual	40mV/min
1SH	Stainless steel	HVOF	Nail polish	Manual	40mV/min
1MP	Mild steel	Plasma	Nail polish	Manual	40mV/min
1MH	Mild steel	HVOF	Nail polish	Manual	40mV/min
1AH	Aluminium	HVOF	Nail polish	Manual	40mV/min
1AP	Aluminium	Plasma	Nail polish	Manual	40mV/min
1S	Stainless steel	None	Nail polish	Manual	40mV/min
1M	Mild steel	None	Nail polish	Manual	40mV/min
1A	Aluminium	None	Nail polish	Manual	40mV/min
2S	Stainless steel	None	Nail polish	Manual	40mV/min
2M	Mild steel	None	Nail polish	Computer	1mV/sec
3S	Stainless steel	None	Nail polish	Computer	1mV/sec
2A	Aluminium	None	Nail polish	Computer	1mV/sec
2MH	Mild steel	HVOF	Nail polish	Computer	1mV/sec
2MP	Mild steel	Plasma	Nail polish	Computer	1mV/sec
4SP	Stainless steel	Plasma	Nail polish	Computer	1mV/sec
2SH	Stainless steel	HVOF	Nail polish	Computer	1mV/sec
2AP	Aluminium	Plasma	Nail polish	Computer	1mV/sec
2AH	Aluminium	HVOF	Nail polish	Computer	1mV/sec
3MH	Mild steel	HVOF	Nail polish	Computer	1mV/sec
4S	Stainless steel	None	Nail polish	Computer	1mV/sec
3A	Aluminium	None	Nail polish	Computer	1mV/sec
2T	Titanium	None	Nail polish	Computer	1mV/sec

Table A2: Summary of working electrodes used in electrochemical experiments.

Designation	**Electrolyte Temperature**	**Start Weight**	**End Weight**	**Start time**	**End time**
1SP	Not taken	Not taken	Not taken	n/t	n/t
2SP	19.2°C	Not taken	Not taken	11.45am	n/t
1T	19.2°C	29.0524g	32.3476g	10.45am	7.45pm
3SP	19.2°C	7.4610g	7.4708g	11.55am	1.15pm
1SH	21.2°C	7.2941g	7.2811g	11.55am	1.17pm
1MP	20.9°C	6.5350g	6.5284g	11.20am	12.45pm
1MH	21.8°C	8.4385g	8.4110g	1145am	1.00pm
1AH	21.5°C	18.6484g	18.6248g	11.40am	12.55pm
1AP	20.8°C	19.8043g	19.8214g	11.00am	12.15pm
1S	21.3°C	5.1849g	5.1597g	12.14pm	1.28pm
1M	21.3°C	6.0924g	6.0163g	11.35am	12.50pm
1A	22.9°C	20.5719g	20.5284g	10.25am	11.40am
2S	23.5°C	7.4139g	7.3919g	12.32pm	1.50pm
2M	22.7°C	6.2512g	6.2166g	12.42pm	1.14pm
3S	23.5°C	8.3192g	8.3112g	11.42pm	1.14pm
2A	24.2°C	20.7585g	20.7655g	1.55pm	2.30pm
2MH	24.5°C	9.6451g	9.6584g	3.50pm	4.25pm
2MP	22.6°C	6.6140g	6.6151g	11.38am	12.11pm
4SP	23.5°C	7.6330g	7.6330g	1.00pm	1.35pm
2SH	24.0°C	7.8665g	7.8544g	2.05pm	2.20pm
2AP	24.6°C	21.4332g	21.4505g	10.30am	11.05am
2AH	23.4°C	19.1992g	19.1881g	11.43am	12.20pm
3MH	23.3°C	8.9668g	8.9479g	11.56am	12.35pm
4S	23.4°C	7.4289g	7.4174g	1.05pm	1.45pm
3A	24.5°C	22.1409g	22.1320g	3.09pm	3.40pm
2T	23.0°C	28.9887g	28.9838g	2.30pm	3.05pm

Table A3: Data taken before and after electrochemical experiments.

Sample type	**Observations**
Stainless steel Plasma	Very slight change in electrolyte colour
Stainless steel HVOF	Corrosion product on bottom of container
Mild steel Plasma	Electrolyte changed colour
Mild steel HVOF	Electrolyte changed colour
Aluminium HVOF	Working electrode bubbled. Bubbling slowed when passivation occurred. Corrosion product dropped directly to bottom in a pile.
Aluminium Plasma	Working electrode bubbled bigger, very slow bubbles. Then small bubbles (but not to the extent of HVOF). Then bubbled out of one (or a few) place. No corrosion product.
Stainless steel	Nail polish appeared to be running, but it was pitting and the corrosion product falling off the working electrode in a steady stream. Deep large pits at top of exposed area.
Mild steel	Corrosion product appeared more and more as the experiment kept going and the electrolyte became more coloured. Exposed area lost thickness universally from the experiment. In the manual experiment the machine errored with RANG OVLD after the current passed 100mA.
Aluminium	Working electrode bubbled. Extensive pitting occurred (the entire surface of the exposed area was covered in pits). Corrosion product was on bottom of electrolyte but also floated on top. In the manual experiment the machine errored with RANG OVLD after the current passed 100mA. Erratic current readings from 840mV onward were observed in the manual experiment (current went up and down)

Table A4: Observations made during the electrochemical experiments.

A (Plasma)		**B (HVOF)**	
Values	**Average**	**Values**	**Average**
Before Spraying			
Lengths (mm)			
99.9		100.4	
99.7	99.8	100.7	100.55
Widths (mm)			
101.5		100.2	
101.2	101.35	99.6	99.9
Thicknesses (mm)			
1.63		1.63	
1.63		1.64	
1.64		1.63	
1.64		1.64	
1.63		1.63	
1.66	1.6383	1.63	1.6333
Weight (g)			
127.587		126.737	
After Spraying			
Thicknesses (mm)			
1.99		1.74	
1.94		1.75	
1.96		1.76	
1.96		1.74	
1.97		1.75	
1.94	1.96	1.75	1.7483
Weight (g)			
141.336		129.059	

Table A5: Measurements taken for density calculations.